

# The Escape of Ionizing Photons from OB Associations in Disk Galaxies: Radiation Transfer Through Superbubbles

James B. Dove<sup>1,2</sup>, J. Michael Shull<sup>1,3</sup>, and Andrea Ferrara<sup>4,5</sup>

<sup>1</sup> CASA, Department of Astrophysical and Planetary Sciences,  
University of Colorado, Campus Box 389, Boulder, CO 80309

<sup>2</sup> Also at Department of Physics,  
Metropolitan State College of Denver, Campus Box 69, Denver, CO 80217

<sup>3</sup> Also at JILA, Campus Box 440, Boulder, CO 80309

<sup>4</sup> Osservatorio Astrofisico di Arcetri, I-50125 Firenze, Italy

<sup>5</sup> JILA Visiting Fellow

## ABSTRACT

By solving the time-dependent radiation transfer problem of stellar radiation through evolving superbubbles within a smoothly varying H I distribution, we estimate the fraction of ionizing photons emitted by OB associations that escapes the H I disk of our Galaxy into the halo and intergalactic medium (IGM). We consider both coeval star-formation and a Gaussian star-formation history with a time spread  $\sigma_t = 2$  Myr. We consider both a uniform H I distribution and a two-phase (cloud/intercloud) model, with a negligible filling factor of hot gas. We find that the shells of the expanding superbubbles quickly trap or attenuate the ionizing flux, so that most of the escaping radiation escapes shortly after the formation of the superbubble. Superbubbles of large associations can blow out of the H I disk and form dynamic chimneys, which allow the ionizing radiation to escape the H I disk directly. However, blowout occurs when the ionizing photon luminosity has dropped well below the association's maximum luminosity. For the coeval star-formation history, the total fraction of Lyman Continuum photons that escape both sides of the disk in the solar vicinity is  $\langle f_{\text{esc}} \rangle \approx 0.15 \pm 0.05$ . For the Gaussian star formation history,  $\langle f_{\text{esc}} \rangle \approx 0.06 \pm 0.03$ , a value roughly a factor of two lower than the results of Dove & Shull (1994b), where superbubbles were not considered. For a local production rate of ionizing photons  $\Psi_{\text{LyC}} = 4.95 \times 10^7 \text{ cm}^{-2} \text{ s}^{-1}$ , the flux escaping the disk is  $\Phi_{\text{LyC}} \approx (1.5 - 3.0) \times 10^6 \text{ cm}^{-2} \text{ s}^{-1}$  for coeval and Gaussian star formation, comparable to the flux required to sustain the Reynolds layer. Rayleigh-Taylor instabilities exist early in the OB association's evolutionary stages, possibly causing the shell to fragment and increasing  $\langle f_{\text{esc}} \rangle$ . However, if a significant fraction of H I is distributed in cold clouds with  $n_{\text{H}} \sim 30 \text{ cm}^{-3}$ ,

$\langle f_{\text{esc}} \rangle$  can be reduced by a factor of  $\sim 2 - 5$  if the cloud properties are similar to “Standard Clouds” with a disk geometry.

*Subject headings:* H II regions — interstellar medium: diffuse ionized gas — radiation transfer: photoionization —

## 1. Introduction

The diffuse, ionized medium (DIM), a.k.a the “Reynolds layer,” has been established to occupy a significant fraction of the interstellar medium (ISM) and to have a vertical scale height of  $\sim 1$  kpc (Mezger 1978; Reynolds 1991a; Reynolds 1991b). It is widely believed that OB associations are the sources of radiation responsible for ionizing the Reynolds layer (Reynolds 1984; Mathis 1986; Bregman & Harrington 1986). It is still unclear how this ionizing radiation is able to travel so far from the OB associations’ immediate vicinity. In a previous paper (Dove & Shull 1994b, hereafter referred to as DS94), we calculated the geometry of diffuse H II regions due to OB associations in the Galactic plane by assuming a three-component model (Dickey & Lockman 1990) for the vertical distribution of hydrogen. For associations producing an ionizing luminosity  $S_0 \gtrsim 3 \times 10^{49} \text{ s}^{-1}$ , we found that the H II regions are “density bounded” in the vertical direction, allowing photons to escape into the halo of our Galaxy. By integrating over the luminosity function of associations,  $dN_a(S_0)/dS_0$  (Kennicutt, Edgar & Hodge 1989; McKee 1997), we estimated that roughly 7% of ionizing photons, corresponding to a number flux  $\Phi_{\text{LyC}} = 2 \times 10^6 \text{ cm}^{-2} \text{ s}^{-1}$ , escape each side of the H I disk layer in the solar vicinity and penetrate the DIM layer. If this radiation is absorbed in the DIM, assumed to lie entirely above the HI layer, the corresponding photoionization rate would be comparable to the recombination rate implied by the  $\text{H}\alpha$  emission measurements (Mezger 1978; Reynolds 1991a; Reynolds 1991b). If roughly one-third of this radiation escapes the Galactic halo, this flux is also consistent with the estimated flux required to photoionize the Magellanic Stream and several high velocity clouds in the solar vicinity (Bland-Hawthorn & Maloney 1999). Rather than assuming a purely diffuse ISM, Miller & Cox (1993) considered the effects of a statistical distribution of small opaque clouds, also decreasing with increasing Galactic height and embedded within the diffuse gas. These authors found that the resulting H II regions are consistent with the observations of dispersion measures and  $\text{H}\alpha$  emission measurements.

Although these results are encouraging, no models to date consider the role of dynamic chimneys and superbubbles produced by the OB associations. These considerations are the focus of this paper. We recently became aware of a preprint on a similar topic (Basu,

Johnstone, & Martin 1999). For an OB association, the stars that produce most of the ionizing radiation have strong stellar winds and form supernovae after their relatively short lifetime. Therefore, shortly after the formation of an OB association, a superbubble will form, with a thin shell behind the shock front excavating a large cavity of hot gas (Weaver et al. 1977; McCray & Snow 1979; McCray & Kafatos 1987; Shull & Saken 1995). For a sufficiently large association, the superbubble can break out of the H I disk, forming a dynamic chimney, where the hot cavity penetrates into the halo (Mac Low & McCray 1988).

As we discuss below, the shells of the expanding superbubbles quickly trap the ionizing radiation, so that no radiation can escape the disk until blowout. After blowout, a large fraction ( $\sim 10\%$  per side) of ionizing radiation can directly escape the disk of the galaxy by propagating through the dynamic chimney. However, this is a viable mechanism for transporting the ionizing radiation only if an appreciable amount of ionizing radiation is still being produced within the cavity after the dynamic chimney has formed. We find that, for both a coeval star formation history or a non-coeval model having a star formation rate given by a Gaussian with a full-width half-maximum  $\sigma_t = 2$  Myr (Massey 1998; Garmany 1998), a small fraction of the ionizing radiation produced by an association over its lifetime is emitted after the time of blowout. Therefore, most of the radiation that escapes the disk does so early in the early stages of the superbubble. Integrating over the luminosity function, we find that the fraction of ionizing photons *currently* being emitted by OB associations that escape each side of the H I disk is  $\langle f_{\text{esc}} \rangle \sim 15\%$  for the coeval star-formation history and  $\langle f_{\text{esc}} \rangle \sim 6\%$  for the Gaussian star-formation history.

The aim of this paper is to predict the fraction of ionizing radiation, emitted by OB associations, that escapes the H I disk of the Galaxy. As discussed above, DS94 assumed that the Reynolds layer lies above the H I layer. Therefore, the question of whether the Reynolds layer is sustained via hot star photoionization is equivalent to whether enough radiation can penetrate through the H I layer. In this paper, we regard this assumption as too simplistic. The Reynolds layer has a scale height of roughly 1 kpc, whereas the H I disk has a scale height of  $\sim 200$  pc (Dickey & Lockman 1990) but extends to at least 1 kpc (Lockman, Hobbs, & Shull 1986). Thus, a significant fraction (e.g.,  $\sim 20\%$ ) of the ionized gas may lie within the H I layer, reducing the flux of ionizing radiation required to escape the H I disk. A self-consistent model, modeling the distribution of the photoionized gas, is not feasible until the density distribution of the hydrogen gas, both within the disk and in the halo, is determined more accurately.

In §2, we discuss our treatment of the evolution of the superbubble and the radiation transfer of ionizing photons emitted by an association through the expanding superbubble and the diffuse ISM of the disk. We also discuss our treatment of the blowout event of the

superbubble, where the cavity evolves into a dynamic chimney. In §3, we determine the time dependence of the fraction of ionizing photons, emitted by a single OB association, that escape the H I disk. Integrating over the luminosity function of OB associations, we determine the fraction of ionizing radiation, currently being emitted by OB associations, that escapes the H I disk. In §4, we discuss key issues not included in our standard model, including shell instabilities, a two-phase ISM, “poisoning” by photoablated gas, and triggered star formation. We then discuss how these effects may alter our results. In §5, we discuss the implications of our results and give our conclusions.

## 2. Radiation Transfer Through an Expanding Superbubble

### 2.1. Evolution of the Superbubble

Consider a large association having  $N_T$  stars in the  $8 - 85 M_\odot$  mass range. Due to the stellar winds from the massive stars and type II supernovae, the association produces a mechanical luminosity,  $L_{\text{mech}}(t)$ , that varies with time. This energy input drives an expanding superbubble. Assuming an initially uniform density distribution of the diffuse ISM, and that all of the swept-up mass resides in a thin shell (the Kompaneets approximation, Kompaneets 1960), the radius,  $R_{\text{sh}}$ , of the cavity is given by (Shull & Saken 1995)

$$\frac{d}{dt} \left[ R_{\text{sh}}^3 \frac{d^2}{dt^2} (R_{\text{sh}}^4) \right] = \frac{6R_{\text{sh}}^2}{\pi\rho} L_{\text{mech}}(t), \quad (1)$$

where the mass density  $\rho = 1.4m_p n_H$ ,  $n_H$  is the number density of hydrogen, and  $m_p$  is the proton mass. For a given time-dependent mechanical luminosity prescription, this equation is integrated numerically using a fourth-order Runge-Kutta algorithm. We note that this formalism is technically valid only for a uniform density distribution, as the shock wave does not evolve with spherical symmetry for non-uniform density distributions. However, as we show in §3, for most association sizes the expanding shell becomes optically thick to the ionizing radiation before the shock has propagated a distance of a disk scale height, within which using a constant density is a good approximation. Therefore, the amount of escaping ionizing radiation is insensitive to the errors produced by neglecting the non-spherical propagation that occurs at large Galactic heights.

The time dependence of the mechanical luminosity depends on the initial mass function (IMF) of stars within an OB association and the star formation history of the association. For this paper, we use the OB association evolution models of Sutherland & Shull (1999), which determine both the mechanical luminosity and the luminosity of ionizing photons as a function of time for individual stars from the latest stellar evolutionary tracks and stellar

atmospheres. These authors used an IMF given by  $dN/dM \propto M^{-(\gamma+1)}$ , where  $\gamma = 1.6$  for the stellar mass range  $8 M_{\odot} \leq M \leq 85 M_{\odot}$  (Garmany 1998), for which all stars eventually become supernovae. The massive star-formation history of the association is given by  $\dot{N}_{\star}(t)$ , with the constraint that  $\int \dot{N}_{\star}(t)dt = N_{\text{T}}$ , where the limits of integration span the entire lifetime of the association. In this paper, we consider two star-formation histories (SFHs): (1) coeval [ $\dot{N}_{\star}(t) \propto \delta(t - t_o)$ ], and (2) noncoeval with a Gaussian distribution [ $\dot{N}_{\star}(t) \propto \exp(-t^2/2\sigma_t^2)$ ]. For the Gaussian SFH, the IMF is assumed to be constant in time.

For each SFH,  $L_{\text{mech}}(t)$  and  $S(t)$  were obtained from Sutherland & Shull (1999). Here, we used a Monte-Carlo simulation to determine the mass distribution of individual associations having a total mass of  $10^4 M_{\odot}$  (corresponding to an average association size of 3000 stars, or roughly  $N_{\text{T}} \sim 300$  massive stars). The average luminosity curves are then normalized, and, for an arbitrary association size, the luminosity curves are given by the product of the normalized curves and  $N_{\text{T}}$ . Note that this formalism ignores all possible deviations about the average luminosities due to statistical fluctuations of the stellar mass distribution of small associations. Sutherland & Shull (1999) found that these fluctuations become significant for  $N_{\text{T}} \lesssim 100$ . However, as shown below, most of the escaping radiation in our Galaxy emanates from associations with  $N_{\text{T}} \gtrsim 100$ , so the importance of the statistical fluctuations of small associations is minor for our purposes. Even if the small associations were important, when calculating the total fraction of escaping photons, we integrate over many associations, so the use of the average luminosities should yield a good approximation.

In Figure 1, we show the mechanical luminosity and the Mach number of the shell as a function of time for an OB association having  $N_{\text{T}} = 200$ , for coeval star-formation history and for a Gaussian star-formation history with  $\sigma_t = 2$  Myr. The Mach number of the shock front is  $\mathcal{M} = v_{\text{sh}}/c_{\text{s}}$ , where the effective sound speed of the medium is

$$c_{\text{s}} = \sqrt{\frac{kT}{\mu_{\text{p}}m_{\text{p}}}(1 + \beta)}. \quad (2)$$

Here,  $k$  is the Boltzmann constant,  $T$  is the temperature of the gas (assumed equal to  $10^4$  K and the shock front is assumed to be isothermal),  $\mu_{\text{p}} = 0.6$ , and  $\beta$  is the ratio of the magnetic pressure plus turbulent pressure to the thermal pressure. As discussed in §2.2, the superbubble is modeled as instantaneously blowing out of the disk and becoming a dynamic chimney when the bubble radius exceeds the transition height,  $Z_{\text{tr}}$ . We assume that  $Z_{\text{tr}}$  is twice the scale height of the H I gas distribution,  $\sigma_{\text{h}}$ . After blowout, the cylindrical radius continues to expand due to conservation of momentum. Once the Mach number reaches unity, the expansion of the cavity is halted.

The fluctuations in the mechanical luminosity arise from supernovae occurring

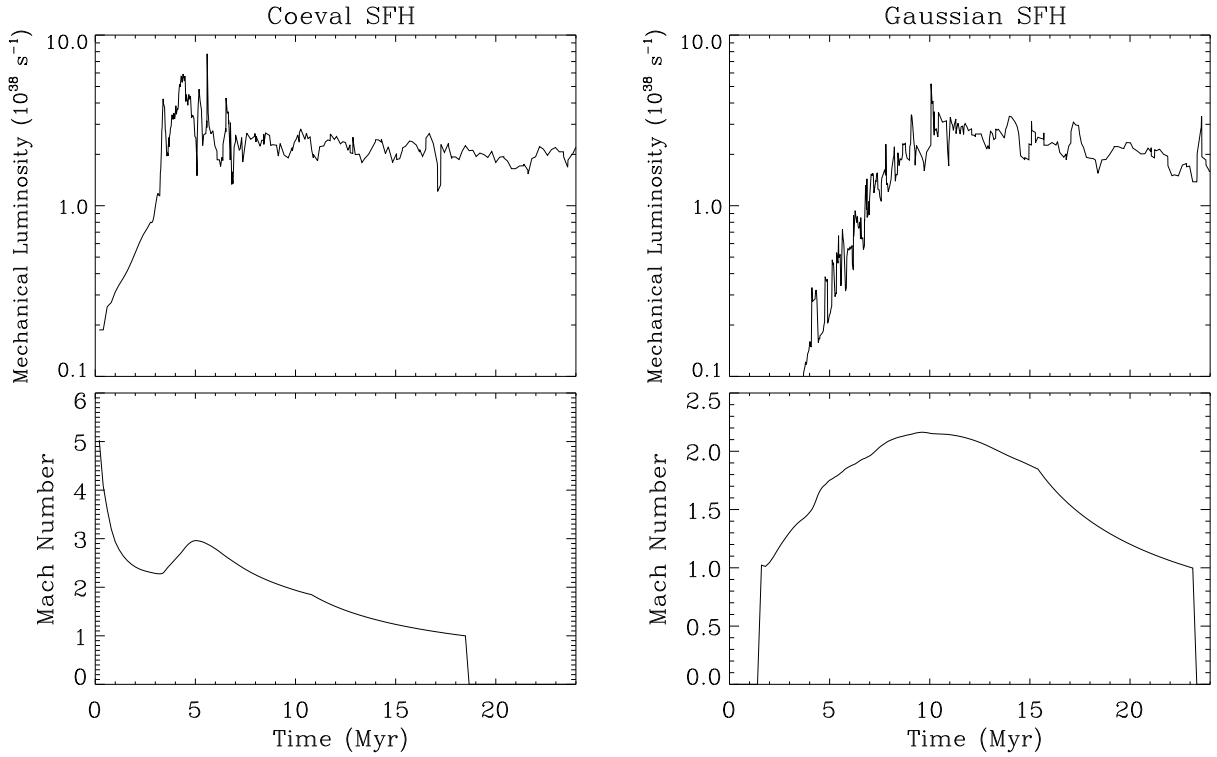


Fig. 1.— Mechanical luminosity of the OB association and Mach number of the shell as a function of time. For the Gaussian SFH,  $\sigma_t = 2$  Myr and the star-formation peak occurs at  $t = 2\sigma_t$ . For both cases,  $N_T = 200$  and  $\beta = 1$ . Blowout occurs when  $t \approx 11$  Myr for the coeval SFH and  $t \approx 16$  Myr for the Gaussian SFH. After blowout, the shell is in the momentum-conserving phase, and the Mach number shown is evaluated at the midplane.

separately in time due to the different lifetimes of individual stars. Although  $L_{\text{mech}}(t)$  is given by the average of several Monte-Carlo simulations, the fluctuations have not been smoothed out.

We note that, for the Gaussian SFH, the Mach number is near zero until 1.3 Myr, when it then rises quickly. This behavior is due to our initial treatment of the bubble growth for low mechanical luminosities. Since we start the simulation at a time  $2\sigma_t$  before the peak star-formation rate, the initial luminosity is small for small associations. In such cases, the Mach number rapidly drops below unity, then subsequently increases as the energy input increases. In reality, the shock front associated with these small associations would stagnate when the ambient pressure of the ISM is equal to the internal pressure of the bubble, causing the Kompaneets approximation to break down. As the proper hydrodynamic treatment of the growth of a stagnated bubble is outside the scope of this paper, we employed the following procedure for approximating the bubble evolution. For each association size, we determine the time at which the mechanical luminosity exceeded  $10^{36}$  erg s<sup>-1</sup>. We then evaluate the Mach number at this time using the solution of equation (1) for a constant luminosity, where the time-averaged luminosity is used. If the Mach number is below unity, we assume that the shock has stagnated, set the shell velocity to zero, and continue integrating equation (1). Although the use of Kompaneet’s equation is not valid for Mach numbers below unity, we argue that the errors introduced are negligible since the time interval for the shell to accelerate to Mach numbers above unity is small relative to the sound-crossing time of the bubble. Therefore, the shell does not diffuse much into the cavity during the stagnation period. Furthermore, during this early interval of the cavity, the photon luminosity of the association is also low, and no radiation escapes the disk of the galaxy regardless of the bubble geometry. Finally, by comparing  $\mathcal{M}(t)$  using this method with results when equation (1) is integrated without intervention, we found that the two were identical for  $t \gtrsim 1.5$  Myr. The only ramification of our stagnation treatment is that smaller associations take longer to blow out of the disk. As discussed in §4.1, the acceleration of stagnated bubbles due to the mechanical luminosity increasing in time can cause Rayleigh-Taylor instabilities to begin at a much earlier stage, compared to the case of constant luminosity, where acceleration occurs at the time of blowout (Mac Low & McCray 1988). This instability may dramatically increase the amount of ionizing radiation that escapes the H I disk.

## 2.2. Superbubble Blowout

For large OB associations that have a sufficiently high mechanical luminosity, superbubbles can blow out of a vertically stratified H I disk, producing dynamic chimneys (Heiles 1979; Tomisaka & Ikeuchi 1986; Mac Low & McCray 1988; Mac Low, McCray & Norman 1989). Blowout occurs if the shell of the superbubble is still supersonic when it reaches a height,  $Z_{\text{acc}}$ , where it begins to accelerate due to decreasing density distribution (Mac Low & McCray 1988). This height depends on the density distribution of the ISM and  $L_{\text{mech}}$ ; for Gaussian or exponential distributions it is  $Z_{\text{acc}} \sim (2 - 3)\sigma_{\text{h}}$  (Mac Low & McCray 1988; Mac Low & Ferrara 1999). For most association sizes and star formation histories, the timescale for reaching  $Z_{\text{acc}}$  is considerably longer than the timescale for propagating from this height into the Galactic halo ( $Z \gtrsim 1$  kpc). Therefore, rather than calculating the exact evolution of the superbubble during blowout, we model the process as an instantaneous transition from a bubble into a dynamic chimney once the shell reaches a transition height  $Z_{\text{tr}} = Z_{\text{acc}}$ . We note that, due to the existence of the H I gas at high  $Z$ , blowout may first occur at heights considerably larger than  $3\sigma_{\text{h}}$  or may not occur at all. In addition, magnetic fields could inhibit blowout (Tomisaka 1998). As discussed below, our results are insensitive to the exact value of  $Z_{\text{tr}}$ , since most ionizing radiation that escapes the disk does so shortly after the formation of the OB association. Therefore, the uncertainties regarding the process of blowout are unimportant for our estimation of the flux of escaping ionizing radiation.

The geometry of the dynamic chimney is approximated as a cylinder, centered on the OB association, with radius  $R_{\text{cy}}$  and height  $Z_{\text{cy}}$ . Since we are only interested in how much ionizing radiation escapes the H I disk of the Galaxy, we do not attempt to model the structure of the superbubble/chimney for heights more than  $\sim 4 - 5$  disk scaleheights ( $\gtrsim 1$  kpc). Numerical simulations of superbubbles blowing out of stratified disks (Tomisaka 1998; Mac Low, McCray & Norman 1989; Mineshige, Shibata & Shapiro 1993) show that a cylinder is a decent approximation for the geometry of the cavity within the H I disk. Above the disk, the shell takes the appearance of a mushroom cloud, with the shell clumping and fragmenting due to Rayleigh-Taylor instabilities. For this paper, we assume that any radiation that reaches a height  $Z_{\text{cy}}$  and is within the dynamic chimney escapes the disk. The question of whether this radiation is absorbed by the “mushroom cap” of the shell or escapes due to the shell having a small covering fraction is outside the scope of this paper. Even if the covering fraction of the “mushroom cap” is not negligible, it is possible that this gas, photoionized by the OB association, is part of the Reynolds layer. Therefore, it is fair to include this radiation when assessing whether the amount of escaping radiation can ionize the DIM.



### 2.3. Ionization Equilibrium of the H II Region

Throughout this paper, we assume that ionization equilibrium is satisfied instantaneously. As discussed in DS94, the ionization front in a Gaussian disk layer will reach a Galactic height  $Z$  in a time

$$\begin{aligned}
 t(Z) = & 15.5 \left[ \frac{\sqrt{\pi}}{4} \operatorname{erf} \left( \frac{Z}{\sqrt{2}\sigma_h} \right) \right. \\
 & \left. - \frac{Z}{2^{3/2}\sigma_h} \exp \left( -\frac{Z^2}{2\sigma_h^2} \right) \right] \\
 & \times \left( \frac{\sigma_h}{0.25 \text{ kpc}} \right)^3 \left( \frac{n_0}{0.3 \text{ cm}^{-3}} \right) S_{49}^{-1} \text{ Myr},
 \end{aligned} \tag{3}$$

where  $S_{49}$  is the photon luminosity in units of  $10^{49} \text{ s}^{-1}$ ,  $\sigma_h$  is the scaleheight of Gaussian disk, and  $n_0$  is the number density of hydrogen in the midplane of the disk. (This equation should replace equation (3) of DS94, whose equation (3) contains an error.) For  $S_{49} = 1$ ,  $\sigma_h = 0.184 \text{ kpc}$ , and  $n_0 = 0.367 \text{ cm}^{-3}$ , the I-front reaches a height  $Z = \sigma_h$  in a time  $t \approx 1.4 \text{ Myr}$  and reaches a height  $Z = 2\sigma_h$  in a time  $t \approx 3.2 \text{ Myr}$ , both relatively small compared to the lifetime of the superbubble. As shown in DS94, ionization equilibrium is reached within a decade or so after the passing of the I-front. [For gas with an ionization fraction  $X \sim 1$ , ionization equilibrium is reached in a time  $\tau \sim (1 - X)/(n_e \alpha_H^{(2)})$ ]. Thus, even though the density distribution of the superbubble is evolving in time (as discussed below), the H II region is determined in a quasi-static fashion.

#### 2.3.1. Geometry of the H II Regions

We assume that the stars of individual OB associations are compactly distributed so that the radiation can be treated as emanating from a point source. We define  $y(t)$  to be the dimming function of the OB association, which relates the time-dependent photon luminosity of Lyman-continuum (LyC) photons and the maximum luminosity via

$$S(N_T, t) = S_0(N_T)y(t). \tag{4}$$

For a point source of ionizing radiation, the H II/H I boundary is given implicitly by

$$\frac{S(N_T, t)}{4\pi\alpha_H^{(2)}} = \int_0^{R_{\text{sh}}} R^2 n_H^2(R, \theta) dR, \tag{5}$$

where  $\theta$  is the angle between the normal of the Galactic disk and the radial unit vector,  $\alpha_H^{(2)}$  is the case-B recombination rate for hydrogen, and  $n_H$  is the number density of hydrogen. Azimuthal symmetry has been assumed.

For the vertical distribution of H I, DS94 considered both the three-component Dickey-Lockman model (Dickey & Lockman 1990) as well as several single Gaussian distributions (with different amounts of dark matter) which were fitted to numerical calculations assuming hydrostatic equilibrium (Dove & Shull 1994a). We found that all models predicted the same fraction of escaping photons within 10%. This Gaussian distribution which most closely resembled the Dickey-Lockman model is given by

$$n_H(Z) = n_0 \exp(-Z^2/2\sigma_h^2), \quad (6)$$

where  $Z$  is the vertical distance above the mid-plane of the disk,  $n_0 = 0.367 \text{ cm}^{-3}$  and  $\sigma_h = 0.184 \text{ kpc}$ . In this paper, we only consider this single-Gaussian distribution.

As the superbubble expands into the diffuse ISM, all of the swept-up mass is assumed to reside in the thin shell. The thickness of the shell,  $\Delta R$ , is given by equating column densities,

$$n_{\text{sh}}(R_{\text{sh}}, \mu) \Delta R = \int_0^{R_{\text{sh}}} n_H(Z) dR, \quad (7)$$

which yields

$$\Delta R = \frac{n_0}{n_{\text{sh}}} \sqrt{\frac{\pi}{2}} \left( \frac{\sigma_h}{\mu} \right) \text{erf} \left( \frac{R_{\text{sh}} \mu}{\sqrt{2} \sigma_h} \right), \quad (8)$$

where  $n_{\text{sh}}$  is the number density within the shell, assumed to be a constant with respect to radius, and  $\mu = \cos \theta$ . Defining the transition radius  $R_{\text{tr}} = R_{\text{sh}} + \Delta R$ , the geometry of the H II region for an OB association with luminosity  $S$ , situated on the mid-plane of the Galaxy, is given implicitly by

$$\begin{aligned} \frac{S}{4\pi\alpha_H^{(2)}} &= \frac{1}{3} n_{\text{sh}}^2(R_{\text{sh}}, \mu) (R_{\text{tr}}^3 - R_{\text{sh}}^3) + \\ &n_0^2 \left( \frac{\sqrt{\pi}}{4} \left( \frac{\sigma_h}{\mu} \right)^3 \left[ \text{erf} \left( \frac{\mu R_{\text{sh}}}{\sigma_h} \right) - \text{erf} \left( \frac{\mu R_{\text{tr}}}{\sigma_h} \right) \right] \right. \\ &+ \frac{\sigma_h^2}{2\mu^2} \left\{ R_{\text{tr}} \exp \left[ - \left( \frac{\mu R_{\text{tr}}}{\sigma_h} \right)^2 \right] - \right. \\ &\left. \left. R_{\text{sh}} \exp \left[ - \left( \frac{\mu R_{\text{sh}}}{\sigma_h} \right)^2 \right] \right\} \right) \end{aligned} \quad (9)$$

The density of this shell is given by the isothermal shock condition for compression in the cool post-shock layer,

$$n_{\text{sh}}(R_{\text{sh}}, \mu) = \mathcal{M}^2 n_{\text{H}}(\mu R_{\text{sh}}). \quad (10)$$

In Figures 2 and 3, we show the time evolution of the geometry of the H II region shortly after the formation of an OB association, for  $N_{\text{T}} = 50$  and  $N_{\text{T}} = 300$ , respectively, assuming coeval star formation. For both association sizes, the H II region is initially density bounded in the vertical direction (see below for discussion of how much radiation escapes the H I disk). As the superbubble expands, the column density of the shell increases. Since the shell has a higher density than the diffuse gas, and therefore a higher recombination rate, the volume of the H II region decreases with time. Eventually, the H II region is radiation bounded even in the vertical direction. For  $N_{\text{T}} = 300$ , a portion of the H I/H II interface lies within the shell for  $t \gtrsim 3.0$  Myr, and by  $t \sim 3.6$  Myr the entire interface is within the shell. The H II region goes from being density limited to radiation limited in a short time interval. For  $N_{\text{T}} = 50$ , the H II region becomes radiation limited at only a slightly earlier time compared to the  $N_{\text{T}} = 300$  association (2.9 Myr compared to 3.5 Myr) even though its photon luminosity is six times lower. This is due to the smaller association having lower shell velocities, causing both a slower accumulation rate of the column density as well as lower gas densities within the compressed shell.

### 2.3.2. Escaping Radiation

If the H II region is density bounded, then some radiation escapes the H I disk. The fraction of ionizing photons that escape along the differential solid angle  $d\Omega(\theta) = \sin \theta \, d\theta d\phi$  is

$$\begin{aligned} f[\theta, S(N_{\text{T}}, t)] &= 1 - \frac{4\pi\alpha_{\text{H}}^{(2)}}{S(N_{\text{T}}, t)} \int_0^{\infty} n_{\text{H}}^2(R, \theta, t) R^2 \, dR \\ &= 1 - \frac{4\pi n_0^2 \alpha_{\text{H}}^{(2)}}{S(N_{\text{T}}, t)} \left\{ \frac{1}{3} \left( \frac{n_{\text{sh}}}{n_0} \right)^2 (R_{\text{tr}}^3 - R_{\text{sh}}^3) + \right. \\ &\quad \left. \left( \frac{\sigma_{\text{h}}}{\mu} \right)^3 \left( \frac{\sqrt{\pi}}{4} \left[ 1 - \text{erf} \left( \frac{\mu R_{\text{tr}}}{\sigma_{\text{h}}} \right) \right] + \right. \right. \\ &\quad \left. \left. \frac{R_{\text{tr}} \mu}{2\sigma_{\text{h}}} \exp \left[ - \left( \frac{\mu R_{\text{tr}}}{\sigma_{\text{h}}} \right)^2 \right] \right) \right\}. \quad (11) \end{aligned}$$

The critical angle,  $\theta_c(S)$ , is the angle at which the H II region is radiation bounded for  $\theta > \theta_c$  and density bounded for  $\theta < \theta_c$ . The critical angle is found by solving  $f(\theta_c, S) = 0$ .

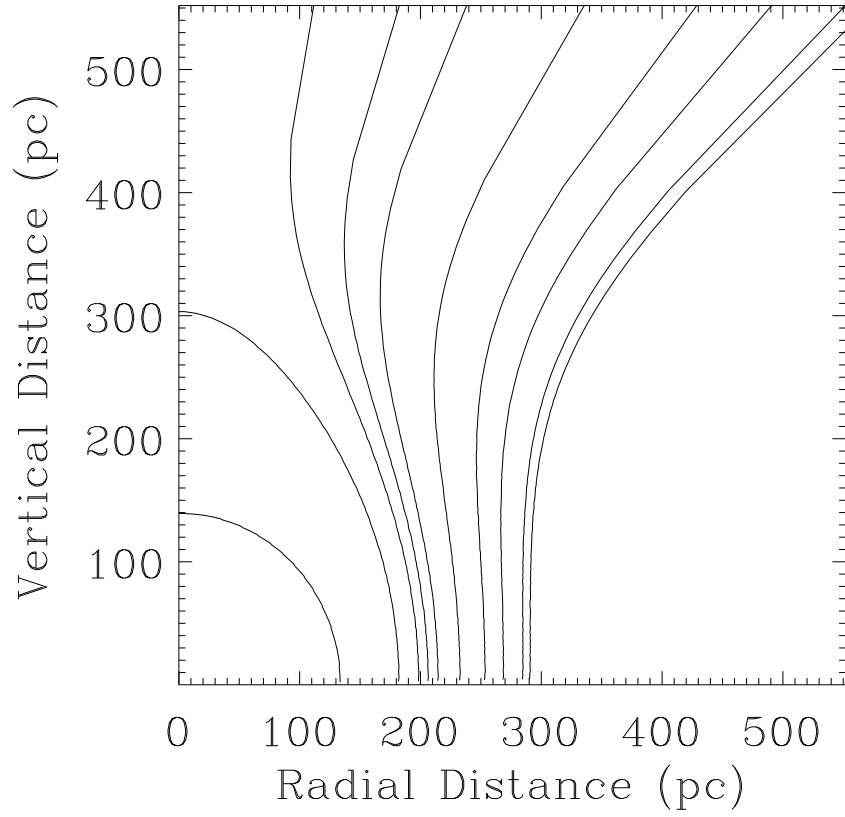


Fig. 2.— Geometry of H II region for several times after the formation of a coeval OB association with  $N_T = 50$  massive stars. From right to left, the time (in Myr) after formation is  $t = 0.0, 1.6, 2.2, 2.4, 2.6, 2.7, 2.8, 2.85, 2.9,$  and  $4.0$ .

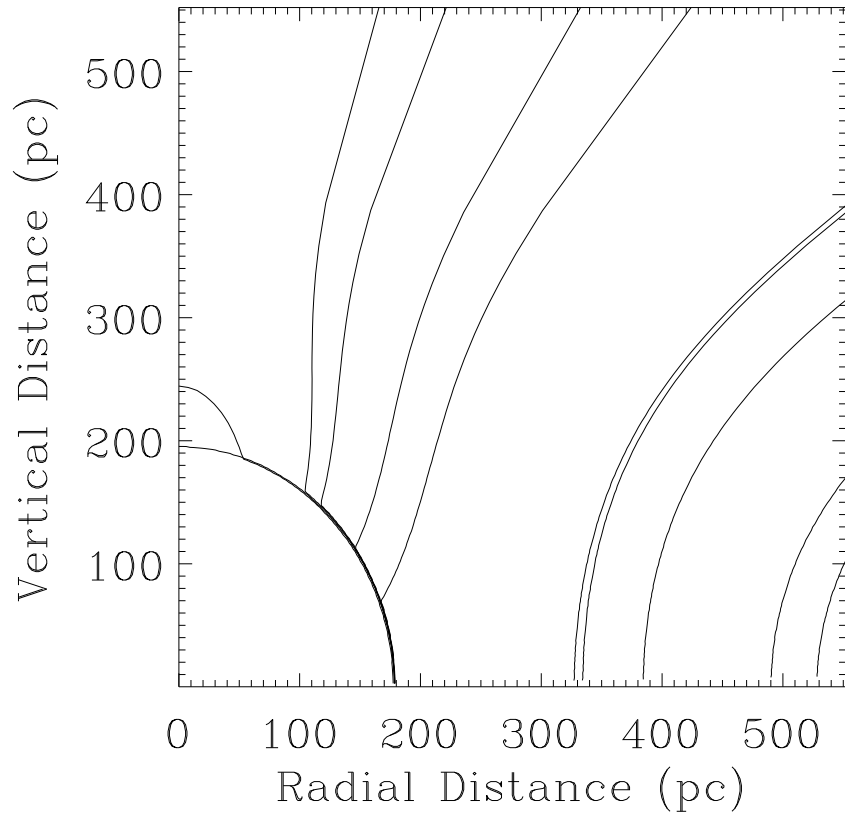


Fig. 3.— Geometry of H II region for several times after the formation of a coeval OB association of size  $N_T = 300$ . From right to left, the time (in Myr) after formation is  $t = 0.0, 2.20, 2.77, 2.93, 3.13, 3.36, 3.40, 3.50, 3.51, 3.54,$  and  $3.61$ .

In contrast to DS94,  $\theta_c$  is time-dependent since both the density distribution and the ionizing luminosity vary with time. Finally, we define the fraction of photons, emitted by a single OB association having size  $N_T$ , age  $t$ , and corresponding luminosity  $S(N_T, t)$ , that escape *each* side of the H I disk to be

$$\eta_{\text{esc}}(N_T, t) = \int_0^{\theta_c} \frac{f(\theta, S)}{4\pi} 2\pi \sin \theta \, d\theta. \quad (12)$$

### 2.3.3. H II Regions for Dynamic Chimneys

For a dynamic chimney with height  $Z_{\text{cy}}$  and cylindrical radius  $R_{\text{cy}}$ , the angle for which  $f(\theta) = 1$  for  $0 \leq \theta \leq \theta_{\text{dyn}}$  is given by  $\theta_{\text{dyn}} = \tan^{-1}(R_{\text{cy}}/Z_{\text{cy}})$ . The procedure for determining the geometry of the H II region and the fraction of escaping photons is similar to that of the superbubbles. The only difference is the treatment of the shell. As with the superbubble, we assume that the density of the shell is  $n_{\text{sh}} = \mathcal{M}^2 n_{\text{H}}$  and that the column density of the shell is equal to the column density of swept-up gas within the cavity. However, for dynamic chimneys, the trajectories of the shell deviate from radial lines since the superbubble evolves from a sphere into a cylindrical cavity. Technically, the column density of the shell for a vertical height  $Z$  would be given by the line integral of the density of the diffuse ISM along the trajectory that leads to the chimney wall at a height  $Z$ . The trajectories can be determined by requiring them to be perpendicular to the surface of the expanding shock wave. For an isothermal atmosphere, Newman et al. (1999) found an analytic solution for the trajectories as a function of time, and, for heights less than a scale height or so, the particle trajectories are found to be roughly radial. For larger heights, the trajectories tend to bend away from the vertical axis and become horizontal near the shell boundary. Therefore, we make the approximation that the streamlines are purely radial for  $Z \leq Z_{\text{tr}}$  and purely horizontal for  $Z > Z_{\text{tr}}$ , where  $Z_{\text{tr}} \sim 2 - 3\sigma_{\text{h}}$ , a free parameter of the model. As discussed below, the results of this paper are insensitive to the value of  $Z_{\text{tr}}$ . With this treatment, for  $Z < Z_{\text{tr}}$ , the shell thickness is given by

$$n_{\text{sh}} \frac{\Delta R(Z)}{\sin \theta} = \int_0^l n_{\text{H}} dR, \quad (13)$$

where  $l = \sqrt{R_{\text{cy}}^2 + Z^2}$  and  $\theta = \tan^{-1}(R_{\text{cy}}/Z)$ . Defining  $R_{\text{sh}} = l$  and  $R_{\text{tr}} = l + \Delta R(Z)/\sin \theta$ , the geometry of the H II region and the fraction of escaping radiation are again given by equations (9) and (12), respectively.

### 3. Results

#### 3.1. Fraction of Escaping Photons as a Function of Time

##### 3.1.1. Coeval Star Formation

In Figure 4 we show the photon luminosity, emitted by a single OB association having  $N_T$  stars, and the luminosity of photons escaping each side of the H I disk as a function of time. Here, the stars are assumed to form coevally. Notice that the fraction of escaping photons,  $\eta_{\text{esc}}(N_T, t)$ , rapidly decreases for  $t \gtrsim 3$  Myr. In fact, for  $N_T = 1000$ , roughly 90% of the time-integrated flux of escaping radiation occurs within the first 2.7 Myr, while only 72% of the time-integrated flux of ionizing radiation has been emitted by this time. The reason for this rapid decrease is that, as the column density of the shell accumulates, the ionizing radiation is very quickly trapped within the shell, causing the fraction of escaping photons to drop to zero. Once the ionization front is trapped within the shell, the fraction of escaping photons remains zero unless the superbubble blows out of the H I disk. (We have not considered shell fragmentation). If blowout occurs, photons can directly escape through the chimney (a small fraction can also escape by penetrating through the upper H II disk), causing  $\eta_{\text{esc}}$  to jump up to  $\sim 10\%$ . However, by the time of blowout, which occurs at  $t \sim 7.0$  Myr for  $N_T = 1000$  and 10.0 Myr for  $N_T = 200$ , the photon luminosity is considerably lower than its peak luminosity (which occurs at  $t \sim 2$  Myr). Therefore, the luminosity of escaping radiation is significantly lower compared to its value for  $t \lesssim 2$  Myr.

##### 3.1.2. Gaussian Star Formation

In Figure 5 we plot the emitted and escaping photon luminosity for case of the noncoeval, Gaussian SFH with  $\sigma_t = 2$  Myr. For  $t = 0$ , the photon luminosity  $S(t)$  is very low, and therefore the fraction of escaping photons is small or even zero, in accordance with the results of our DS94. As the luminosity increases,  $\eta_{\text{esc}}$  increases until the shell of the superbubble becomes thick enough that the shell-integrated recombination rate approaches the photoionization rate. Since the shell expands more slowly compared to the coeval SFH (having the same value of  $N_T$ ), the column density of the shell does not increase as quickly. In addition, due to the lower Mach number of the shock front, the shell density is lower than that of the coeval SFH. For these two reasons,  $\eta_{\text{esc}}$  does not fall off in time as quickly as in the coeval case after it reaches its peak value. Nevertheless, the shell does attenuate significantly the flux of escaping radiation. In Figure 6, for  $N_T = 200$ , we compare the flux of escaping radiation as a function of time with that for the case where no dynamics are

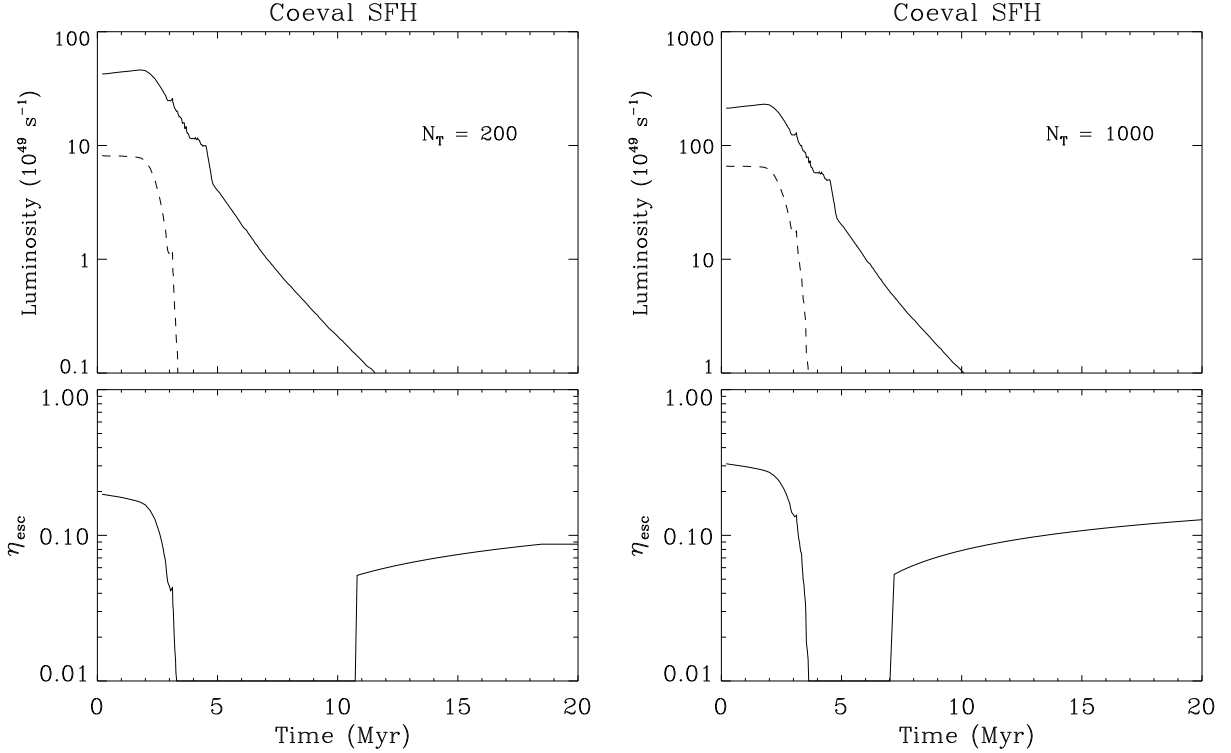


Fig. 4.— Photon luminosity emitted by a single OB association (solid line) and the luminosity of photons escaping each side of the H I disk (dashed line) for coeval star-formation. Also shown is the fraction of photons emitted that escape,  $\eta_{\text{esc}}(N_{\text{T}}, t) = S_{\text{esc}}(t)/S(t)$ . Here,  $Z_{\text{tr}} = 2\sigma_{\text{h}}$ , the cavity height is  $Z_{\text{cy}} = 4\sigma_{\text{h}}$ , and  $\beta = 1$ . The I-front is trapped within the shell during the time interval where  $\eta_{\text{esc}} = 0$ . After blowout,  $\eta_{\text{esc}}$  suddenly increases even though the photon luminosity of the association is relatively low at these times.



considered (e.g., as done by DS94 but using the time-dependent photon luminosity). For  $t \gtrsim 5$  Myr, the shell becomes efficient in reducing the escaping flux. Therefore, as with the coeval SFH, most of the escaping radiation escapes early, within a short time interval relative to the lifetime of the OB association. The time-integrated flux of photons that escape the disk after blowout is considerably small relative to the lifetime-integrated flux. For example, for  $N_T = 1000$ , fewer than 3% of the photons that escape the disk over the lifetime of the association escape after blowout (while fewer than 4% of the photons emitted by the association are produced after blowout). For  $N_T = 200$ , approximately 1% escape after blowout. These values are not much different than for the coeval SFH. The reason for this insensitivity is that as  $\sigma_t$  is increased ( $\sigma_t = 0$  for coeval star-formation), the blowout timescale is also increased. Thus, even though there are more stars alive at longer times for noncoeval SFHs, there are still relatively few alive at the time of blowout.

### 3.2. Time Integrated Fraction of Escaping Photons

The time-integrated fraction of escaping photons for each side of the H I disk by an association of size  $N_T$  is given by

$$\langle \eta_{\text{esc}}(N_T) \rangle = \frac{\int_0^{\infty} \eta_{\text{esc}}(N_T, t) S(N_T, t) dt}{\int_0^{\infty} S(N_T, t) dt}. \quad (14)$$

In Figure 7 we plot  $\langle \eta_{\text{esc}}(N_T) \rangle$  for both the coeval SFH and the noncoeval Gaussian star-formation model. For reference, the maximum photon luminosity of an association over its lifetime is  $S_0(N_T) = 0.231 N_T (10^{49} \text{ s}^{-1})$  for coeval star-formation and  $S_0(N_T) = 0.122 N_T (10^{49} \text{ s}^{-1})$  for the Gaussian SFH. Note that  $\langle \eta_{\text{esc}} \rangle$  is smaller for all values of  $N_T$  for the Gaussian SFH. There are several reasons for this difference. One reason is that, for a given value of  $N_T$ , the Gaussian SFH has a peak photon luminosity that is roughly a factor of two smaller than that of the coeval model. Therefore, even if the shell structures of the superbubble were identical during the interval of maximum luminosity, the maximum value of  $\eta_{\text{esc}}$  for the Gaussian model would be smaller since  $\eta_{\text{esc}}$  increases with increasing photon luminosity (DS94). In addition, the luminosity profile  $S(t)$  for the coeval model is much more peaked, with  $\sim 70\%$  of its lifetime-integrated luminosity emitted within the first 2.5 Myr, compared to the relatively broad distribution of  $S(t)$  for the Gaussian SFH. Thus, since  $\langle \eta_{\text{esc}} \rangle$  is weighted by  $S(t)$ , and  $\eta_{\text{esc}}(N_T)$  is near its peak value while  $S(t)$  is near its peak value, the coeval SFHs yield higher values. Finally, for coeval SFHs, the peak of  $S(t)$  occurs shortly after the formation of the association, before the formation of a significant superbubble shell, allowing these photons to escape more easily.

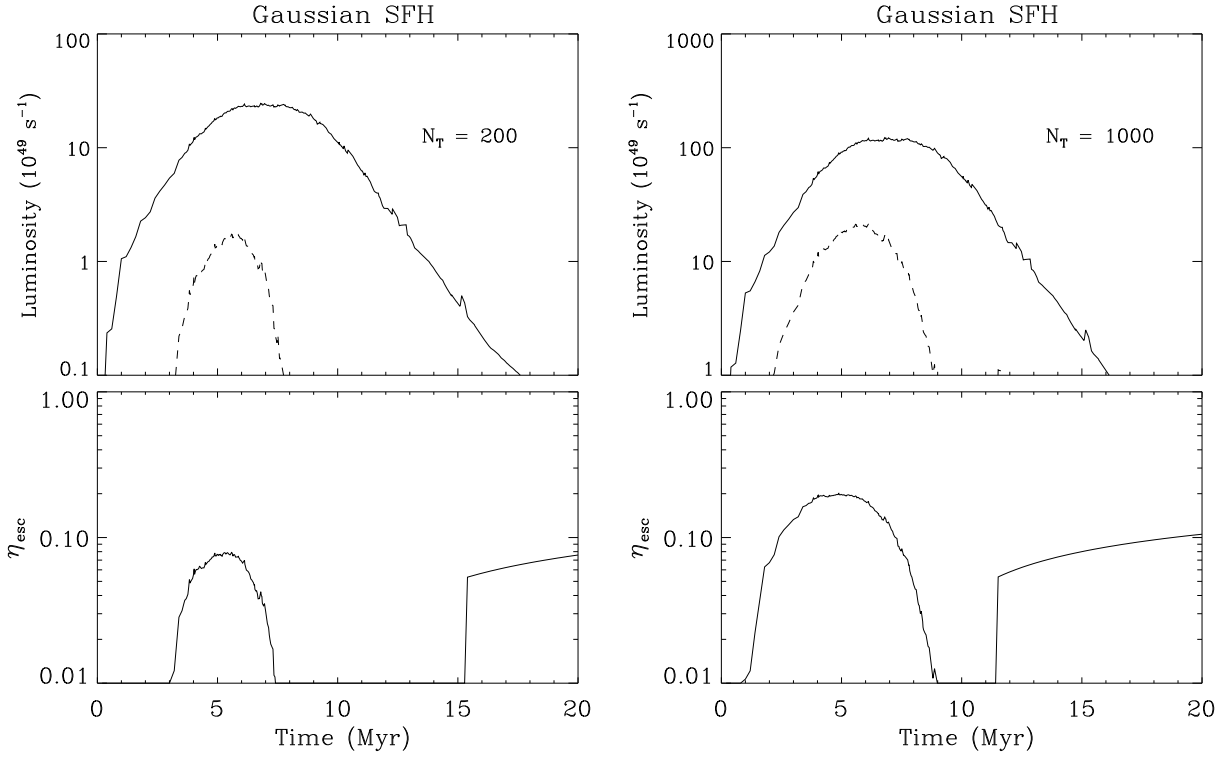


Fig. 5.— Photon luminosity emitted by a single OB association (solid line) and the luminosity of photons escaping each side of the H I disk (dashed line) for a Gaussian SFH with  $\sigma_t = 2$  Myr. Also shown is the fraction of emitted photons that escape,  $\eta_{\text{esc}}(N_T, t) = S_{\text{esc}}(t)/S(t)$ . Here,  $Z_{\text{tr}} = 2\sigma_h$ ,  $Z_{\text{cy}} = 4\sigma_h$ , and  $\beta = 1$ .

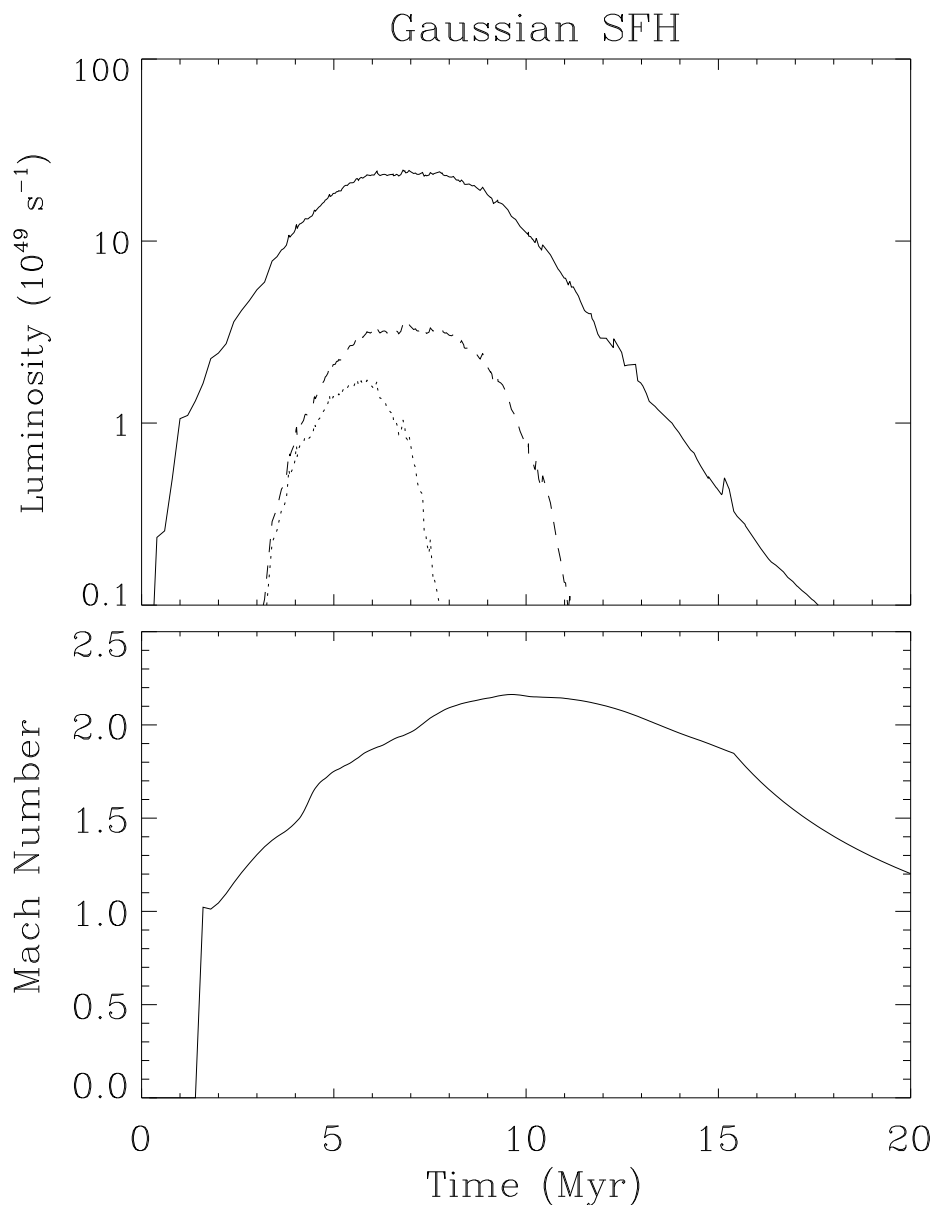


Fig. 6.— Photon luminosity emitted by a single OB association (solid line) of size  $N_T = 200$  and the luminosity of photons escaping each side of the H I disk (dotted line) for a Gaussian SFH with  $\sigma_t = 2$  Myr. Also shown is the luminosity of escaping photons for the case where the dynamics of the bubble is not considered (dashed line). The bottom panel shows the Mach number of the shock front as a function of time. Due to the high density of the evolving shell, the luminosity of escaping radiation is reduced for  $t \gtrsim 4$  Myr.

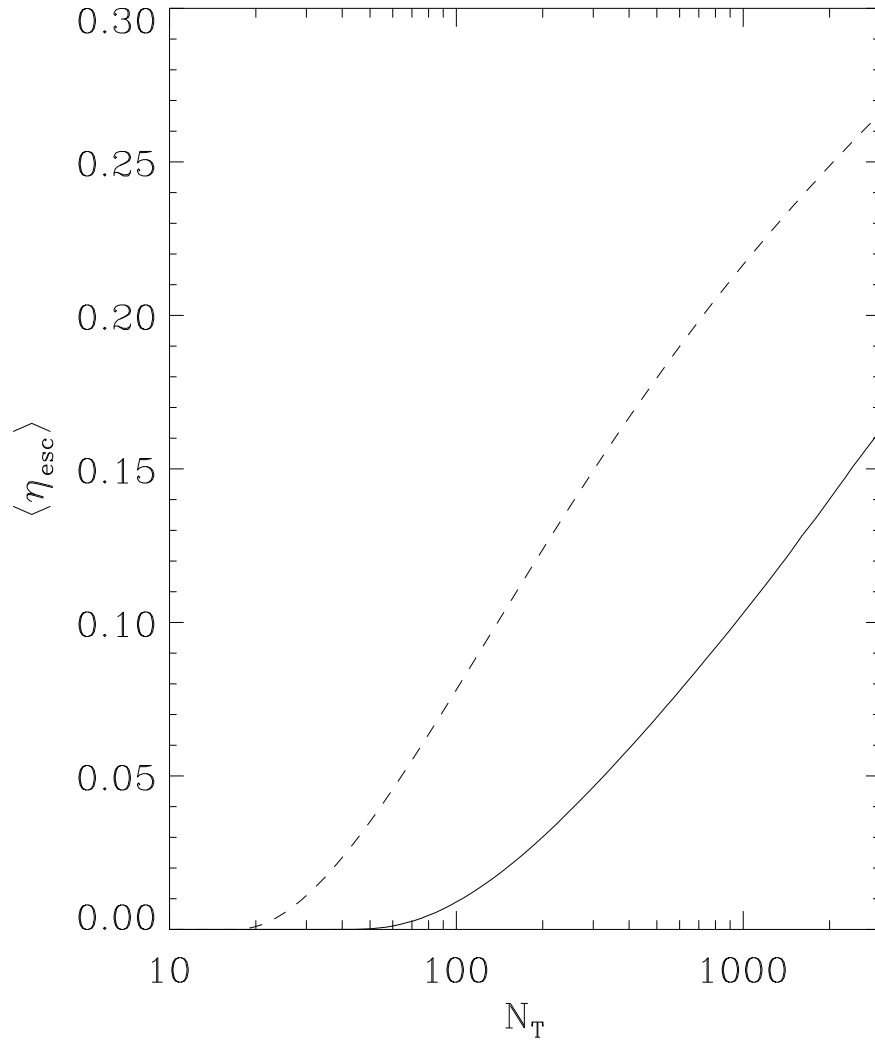


Fig. 7.— Time-integrated fraction of escaping photons as a function of association size  $N_{\text{T}}$ . Here,  $Z_{\text{tr}} = 2\sigma_{\text{h}}$ ,  $Z_{\text{cy}} = 4\sigma_{\text{h}}$ , and  $\beta = 1$ . Solid line: Gaussian SFH,  $\sigma_{\text{t}} = 2$  Myr. Dashed line: Coeval SFH.

### 3.3. Fraction of Escaping Ionizing Photons

We now discuss the fraction of photons, currently being emitted by OB associations of all ages and sizes, that escape the H I disk of the Galaxy.

#### 3.3.1. Luminosity Function

We assume a constant formation rate,  $\dot{N}_{\text{as}}$ , of associations per unit area in our Galaxy. The probability of a new association having a peak luminosity  $S_0$  [recall that  $S(N_{\text{T}}, t) = S_0(N_{\text{T}})y(t)$ ] is given by the implicit association luminosity function,  $dN/dS_0$ . Therefore, during a small time interval  $\delta t$ , the number of associations that will eventually have a peak luminosity  $S_0$  is  $\delta N(S_0) = \dot{N}_{\text{as}} dN/dS_0 \delta t$ . The number density ( $\text{kpc}^{-2} \text{s}^{-1}$ ) of associations observed today as a function of luminosity,  $dN_{\text{as}}(S)/dS$ , is related to the implicit luminosity function via

$$\frac{dN_{\text{as}}(S)}{dS} = \int_{t_1(S)}^{t_2(S)} \dot{N}_{\text{as}} \frac{dN}{dS_0} [S_0 = S/y(t)] dt. \quad (15)$$

Here,  $t_2(S)$  is given by  $t_2 = y^{-1}(S/S_2)$ , where  $y^{-1}$  is the inverse function of  $y(t)$ , and  $t_1$  is given by

$$t_1 = \begin{cases} 0 & : S \geq S_1 \\ y^{-1}(S/S_1) & : S < S_1. \end{cases} \quad (16)$$

If the dimming function  $y(t)$  is multi-valued, then  $t_2$  and  $t_1$  (for  $S < S_1$ ) are determined from its maximum values.

The observed luminosity function, from H $\alpha$  measurements of all known H II regions in 30 nearby spiral and irregular galaxies, is given by  $dN_{\text{as}}(S)/dS \propto S^{-\Gamma}$  for  $S_1 \leq S \leq S_2$ , where  $\Gamma = 2.0 \pm 0.5$  (Kennicutt, Edgar & Hodge 1989; Banfi et al. 1993; Rozas, Beckman & Knapen 1996, and references therein). McKee (1997) finds a similar result from studying Galactic H II regions. See DS94 for a discussion regarding the uncertainty of the upper and lower limits of the luminosity function. Assuming  $dN/dS_0 \propto S_0^{-\Gamma}$  with  $\Gamma \gtrsim 1$ , the corresponding  $dN_{\text{as}}(S)/dS$  is close to a pure power law with the same power-law index, with deviations first occurring at  $S \sim S_2$ . Therefore, for the remainder of this paper, unless otherwise stated, we assume that the intrinsic luminosity function is a power law with  $\Gamma = 2$ .

A better understanding of the relationship between the implicit luminosity function and the observed luminosity function can be obtained by considering an example with

a simple analytical dimming function,  $y(t)$ . Assume  $y(t) = \exp(-t/\tau)$  and the implicit luminosity function  $dN/dS_0 = N_0 S_0^{-\Gamma}$ . Then, for  $S > S_1$ ,

$$\begin{aligned}
 \frac{dN_{\text{as}}(S)}{dS} &= \int_{t_1(S)}^{t_2(S)} \dot{N}_{\text{as}} \frac{dN}{dS_0}(S_0 = S/y(t)) dt & (17) \\
 &= \dot{N}_{\text{as}} N_0 \int_0^{t_2} \left( \frac{S}{y(t)} \right)^{-\Gamma} dt \\
 &= \dot{N}_{\text{as}} N_0 S^{-\Gamma} \int_0^{t_2} \exp(-\Gamma t/\tau) dt \\
 &\propto S^{-\Gamma} [1 - \exp(-\Gamma t_2/\tau)]. & (18)
 \end{aligned}$$

Here,  $t_2 = y^{-1}(S/S_2) = -\tau \ln(S/S_2)$ , so finally we have

$$\frac{dN_{\text{as}}(S)}{dS} \propto S^{-\Gamma} \left[ 1 - \left( \frac{S}{S_2} \right)^{\Gamma} \right]. \quad (19)$$

Therefore for  $S > S_1$  and  $S \ll S_2$ ,  $dN_{\text{as}}/dS \propto S^{-\Gamma}$ . The larger the value of  $\Gamma$ , the closer  $S$  must be to  $S_2$  for appreciable differences to occur between the intrinsic and observed luminosity functions. For  $\Gamma = 2$ , a 10% difference between the two functions first occurs when  $S/S_2 > 0.32$ . Since the range of association luminosities is several orders of magnitude, and the value of  $S_2$  is very uncertain, we regard this discrepancy as negligible. Note that the reason for any differences between the two luminosity functions is due to our prescription that the implicit luminosity function is truncated at  $S_2$ . Physically, as  $S$  approaches  $S_2$ , only the largest associations recently formed can contribute to the luminosity function, causing the observed luminosity function to drop to zero as  $S$  reaches  $S_2$ . Also note that the difference between the two luminosity functions is independent of the functional form of the dimming function.

### 3.3.2. Production Rate and Escaping Rate of Ionizing Photons

The current production rate of ionizing photons (# per unit area per unit time) is given by

$$\Psi_{\text{LyC}} = \int_0^{S_2} S \frac{dN_{\text{as}}}{dS} dS. \quad (20)$$

Substituting the expression for the observed luminosity function in terms of the implicit luminosity function [equation (15)], we find,

$$\Psi_{\text{LyC}} = \dot{N}_{\text{as}} \int_0^{S_2} S \int_{t_1}^{t_2} \frac{dN}{dS_0}(S_0 = S/y(t)) dt dS. \quad (21)$$

The flux of photons escaping from each side of the H I disk is given by

$$\Psi_{\text{esc}} = \dot{N}_{\text{as}} \int_0^{S_2} S \int_{t_1}^{t_2} \eta_{\text{esc}}(S, t) \frac{dN}{dS_0} [S_0 = S/y(t)] dt dS. \quad (22)$$

Here,  $\eta_{\text{esc}}(S, t)$  is the fraction of photons that escape each side of the H I disk emitted by an association of size  $N_{\text{T}}$ , where the peak luminosity of this association is  $\max[S(N_{\text{T}}, t)] = S_0(N_{\text{T}})$ . By computing a two-dimensional grid of  $\eta_{\text{esc}}(N_{\text{T}}, t)$  using the methods outlined in §2.3.2, we integrate equation (22) for the two star-formation scenarios. For given values of  $S$  and  $t$ , an interpolation routine was used to find the corresponding value of  $N_{\text{T}}$ , such that  $\eta_{\text{esc}}(S, t) = \eta_{\text{esc}}[N_{\text{T}}(S, t), t]$ . Finally, the total fraction of photons, currently being emitted, that escape both sides of the H I disk is

$$\langle f_{\text{esc}} \rangle = 2 \frac{\Psi_{\text{esc}}}{\Psi_{\text{LyC}}}. \quad (23)$$

We find that  $\langle f_{\text{esc}} \rangle \sim 12\%$  for the coeval SFH and  $\langle f_{\text{esc}} \rangle \sim 6\%$  for the Gaussian SFH. In Figure 8, we show how  $\langle f_{\text{esc}} \rangle$  depends on the model parameters. For reasons given in §3.2,  $\langle f_{\text{esc}} \rangle$  for the Gaussian SFH is considerably lower than that for the coeval SFH. By far,  $\langle f_{\text{esc}} \rangle$  is most sensitive to the power-law index of the luminosity function,  $\Gamma$ . This sensitivity arises because most of the escaping radiation comes from the relatively few large associations with  $N_{\text{T}} \gtrsim 100$ ; small changes in  $\Gamma$  cause rather large changes in the relative number of these large associations. For the coeval SFH,  $\langle f_{\text{esc}} \rangle$  is insensitive to the magnetic field (the parameter  $\beta$ ). As the superbubble expands, the column density of the shell increases quickly, causing  $\eta_{\text{esc}}(S, t)$  to drop to zero very quickly even for strong magnetic fields. For the Gaussian SFH, the superbubble expands more slowly, and different values of  $\beta$  cause the shell to trap the ionization front at different times. Since this trapping of the I-front occurs near the peak of  $S(t)$ ,  $\langle f_{\text{esc}} \rangle$  is more sensitive to  $\beta$ . Lastly, we do not plot how  $\langle f_{\text{esc}} \rangle$  depends on the parameters involved with the superbubble blowout (e.g.,  $Z_{\text{tr}}$  and  $Z_{\text{cy}}$ ), as we found that varying these parameter over a range between  $\sigma_{\text{h}}$  and  $4\sigma_{\text{h}}$  corresponded to a relative change of  $\langle f_{\text{esc}} \rangle$  less than 1%. This insensitivity occurs because most emitted and escaping photons occur early after the formation of the association.

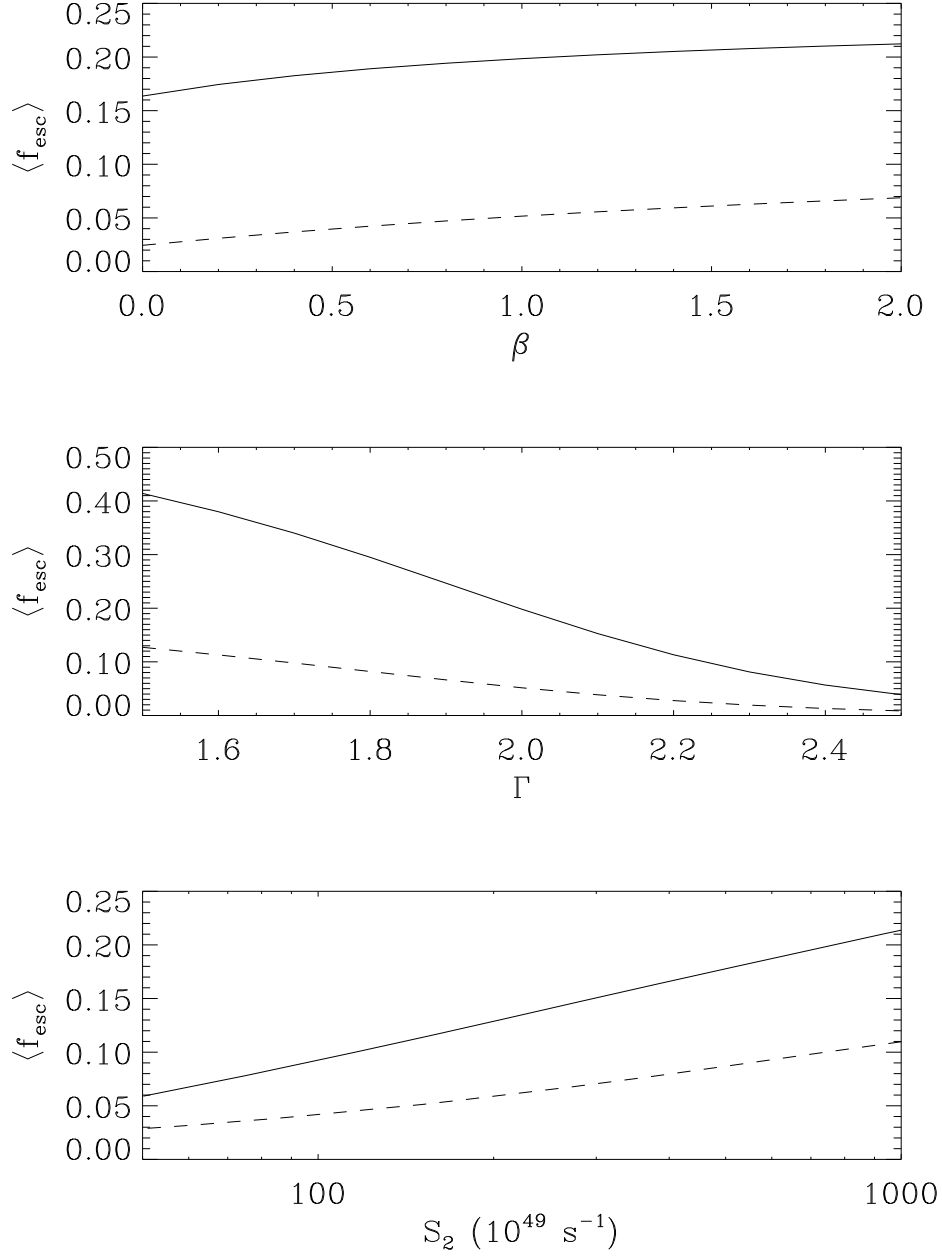


Fig. 8.— Fraction of Ly $\alpha$  photons, currently being emitted, that escape each side of the H I disk. Solid line: coeval SFH. Dashed line: Gaussian SFH with  $\sigma_t = 2$  Myr. Top panel:  $\Gamma = 2$  ( $dN/dS_0 \propto S_0^{-\Gamma}$ ) and the maximum association size is  $N_T = 3200$  (corresponding to  $S_2 = 7.4 \times 10^{51} \text{ s}^{-1}$  for the coeval star formation history and  $S_2 = 3.9 \times 10^{51} \text{ s}^{-1}$  for the Gaussian SFH). Middle panel:  $\beta = 1$ , and the range of association sizes is the same as given above. Bottom panel:  $\Gamma = 2$  and  $\beta = 1$ . For all models,  $Z_{\text{tr}} = 2\sigma_h$ .



## 4. Complexities to the Model

We now discuss the key issues not included in our standard model. We then discuss how these effects may alter our results.

### 4.1. Shell Instabilities

As discussed above, the presence of a thick neutral shell of cool, shocked ISM produced by multiple supernova explosions is quite effective in absorbing the radiation coming from the OB association. This process significantly reduces the fraction of photons able to escape into the galactic halo until blowout takes place. At that stage, the previously decelerating shell is suddenly accelerated and the interface between the dense shell and the hot cavity gas becomes Rayleigh-Taylor (R-T) unstable. The nonlinear development of such instability induces fragmentation of the shell into a number of clumps, through which the photons can percolate and almost freely escape into the halo. This process generally occurs relatively late (or not at all), when the radiative flux has already decreased by a considerable amount due to the aging of the parent OB association. It is thus worthwhile to investigate if the fragmentation process driven by R-T or other instabilities can take place before blowout, consequently increasing  $\langle f_{\text{esc}} \rangle$ .

There are at least three types of instabilities that could affect the shell at the beginning or during the pressure-driven radiative (PDR) phase: 1) dynamical, 2) Rayleigh-Taylor and 3) gravitational. To assess the importance of these processes, it is necessary to discuss in more detail the development of the shell structure for SN bubbles. We restrict our discussion to uniform ambient gas density, which is a reasonable approximation to study the pre-blowout phase. The structure of a wind-blown bubble (the energy injection by multiple SNe can be well approximated as a continuous process) is constituted by a reverse (“wind”) shock propagating back into the wind, which is under most conditions adiabatic, and an “ambient” shock propagating into the surrounding medium; the two shocks are separated by a contact discontinuity. Initially, the ambient shock is also adiabatic and its radius increases with time as  $t^{3/5}$ . However, when the cooling time of the shocked ambient gas becomes of the order of the age of the bubble, the ambient shock becomes radiative and the shocked ambient gas collapses into a thin shell.

The shell-formation phase is characterized by violent dynamical instabilities which tend to amplify the perturbation due to classical thermal instability in the catastrophically cooling shocked ambient gas. Are these instabilities able to disrupt the shell soon after its formation? At least three different dynamical instabilities may arise in the thin, cool shell:

nonradial oscillations of the radiative shock (Bertschinger 1986), the nonlinear thin-shell (NTSI) instability arising when the shell is bounded by two radiative shocks (Vishniac 1983), and the pressure-driven thin-shell overstability (PDTSO) found in a shell bounded by a high thermal pressure on one side and by a radiative shock on the other (Vishniac 1994). These dynamical instabilities may produce considerable distortions in the shell, often showing nonradial oscillations. The main difference between the latter two instabilities is that while the NTSI grows exponentially, the PDTSO only grows with a power-law rate. Recent numerical simulations (MacLow & Norman 1993; Blondin et al. 1998) have shown that the PDTSO is probably the most dangerous instability, especially for superbubbles where the wind shock is adiabatic rather than radiative for a large fraction of its evolution. However, the PDTSO works only for the time during which the Mach number of the shell is larger than  $\sim 3$ . As the PDTSO grows with time as  $t^s$  with  $s \approx 1/2$ , whereas the shock velocity decreases as  $t^{-2/5}$  (see equation [24] below) in the radiative phase, amplifications  $\lesssim 30$  are typically possible, i.e. the overstability saturates. The above numerical studies concluded on this basis that fragmentation of the shell due to these instabilities is unlikely, although Blondin et al. (1998) emphasize that in a denser ISM the shock enters the radiative phase at a higher Mach number, thus allowing for a longer growth time of the instability.

Even if the shell can survive dynamical instabilities, it can be fragmented by R-T instabilities generated *before* blowout. As the radiative bubble expands, its pressure drops and eventually becomes equal to the that of the ISM. In this case, the wind shock stalls, but the shocked wind is still adiabatic and forces the shell to continue its expansion. However, the expansion rate is now so slow that the acceleration of the shell is dominated by the galactic gravitational field. Thus, the polar region of the shell will be R-T unstable even in the absence of a blowout. We calculate the time at which the pressure-confined phase occurs (and hence the R-T instability starts to grow) as follows. For constant luminosity, the evolution of the shell radius in the radiative phase is given by (Castor, McCray & Weaver 1975; Weaver et al. 1977; Ostriker & McKee 1988)

$$R(t) \simeq 66 \left( \frac{L_{38}}{n_0} \right)^{1/5} t_6^{3/5} \text{ pc} \quad (24)$$

where  $L_{38} \equiv L/(10^{38} \text{ erg s}^{-1})$  is the wind mechanical luminosity,  $n_0$  is the ambient gas number density, and  $t_6 \equiv t/(10^6 \text{ yr})$ . From the pressure balance condition  $\dot{R}^2 = c_s^2$ , where  $c_s$  is the ISM effective sound speed, this transition occurs at

$$t_p \simeq 3 \times 10^7 \left( \frac{L_{38}}{n_0 c_{s,10}^5} \right)^{1/2} \text{ yr} \quad (25)$$

where  $c_{s,10} \equiv c_s/(10 \text{ km s}^{-1})$  is the ISM effective sound speed. The growth time of the R-T

instability on spatial scales  $\lambda_s \sim \sigma_h$  is

$$t_{\text{RT}} \simeq \left[ \frac{2\pi g (\Delta - 1)}{\lambda_s (\Delta + 1)} \right]^{-1/2} \simeq \left( \frac{2\pi g}{\lambda_s} \right)^{-1/2} \sim 1 \text{ Myr} \quad (26)$$

if the density contrast between the shell and the hot cavity gas  $\Delta \equiv n_s/n_h \gg 1$  and  $\langle g \rangle = 10^{-8} \text{ cm s}^{-2}$ . As  $t_{\text{RT}}$  is much shorter than  $t_p$ , the shell is fragmented soon after it enters the pressure-confined phase. For the case of a Gaussian SFH, the mechanical luminosity is initially very low, causing the shock to stagnate much earlier than the constant-luminosity case.

In addition, the shell can be re-accelerated early in its evolutionary stage shortly after the first supernovae of the association due to the sudden increase in the mechanical luminosity. We have numerically evaluated  $\langle g \rangle$  due to this process assuming the Kompaneets approximation is valid, and find that the product of  $\langle g \rangle$  and the duration of the re-acceleration (typically  $\sim 1 - 4 \text{ Myr}$ ) is  $\sim 5$ . Thus, the growth of the instability is moderately non-linear. A more detailed study of this process, including the role of poisoning, will be given in Dove, Ferrara, & Shull (1999). Therefore, in contrast to the case of a constant mechanical luminosity, the shell can be R-T unstable before blowout. In this case, a fragmenting shell would allow a higher amount of ionizing radiation to escape the H I disk since fragmentation occurs during the time interval in which the photon luminosity of the association is near its peak value.

The shell might also be fragmented by a gravitational instability. Several studies have investigated this possibility, both under interstellar (Elmegreen & Lada 1977; McCray & Kafatos 1987; Voit 1988) and intergalactic conditions (Ostriker & Cowie 1981; Couchman & Rees 1986). Here, we simply state the the growth time of the most unstable mode is

$$t_G \simeq \frac{3c_s^2}{\pi G \rho_0 R(t)} = 2 \times 10^7 L_{38}^{1/8} n_0^{-1/2} \text{ yr}. \quad (27)$$

Again, we see that this mechanism is able to fragment the shell on time scales of interest and similar to the ones found for the R-T instability. We conclude that, even in the absence of blowout, fragmentation of the shell is likely about  $3 \times 10^7 \text{ yr}$  after the beginning of the energy injection.

Even if the shells of superbubbles do not blow out, do they fragment while the OB association is still producing ionizing photons? Simple conditions on the occurrence of blowout have been derived in different contexts by Mac Low & McCray (1988) and Mac Low & Ferrara (1999). Neglecting the role of magnetic fields, Koo & McKee (1992) studied in detail the case for the Milky Way and concluded that the blowout requires  $L_{38} \gtrsim 4$ . For a marginally confined bubble, we find from equation (25) and equation (27)

that  $t_p \approx 6 \times 10^7$  yr and  $t_G \approx 2.4 \times 10^7$  yr for the R-T and the gravitational instability, respectively. Note that, as  $L_{38}$  is decreased, fragmentation occurs earlier in time. Thus, even bubbles that do not blow out of the disk can fragment on time scales short enough that at least some ionizing photons escape. Determining the covering fraction of the fragmented clumps is outside the scope of the present estimates and will require numerical simulations of the fragmentation process. As a final caveat, we stress that a dynamically important magnetic field could qualitatively modify the above conclusions by suppressing some of the instabilities (Tomisaka 1998) and by introducing new ones.

## 4.2. Clumpiness of the Diffuse H I Gas

Although our models assume that, outside the superbubbles, the neutral gas is distributed diffusely, there is observational evidence that a significant fraction of the gas is in cold H I clouds, with densities much larger than the space-averaged density. Due to the higher recombination rates, these clouds modify our radiation-transfer results and therefore merit some consideration. Since most radiation that escapes the H I disk comes from young OB associations, with shells having small column densities, we considered the ramifications of a clumpy medium by ignoring the effects of evolving superbubbles. A more proper treatment would consider the time-dependent evolution of the clouds due to passage of the shell of the superbubble as well as the expansion and evaporation of the clouds after being photoionized.

As an approximate model, we let a mass-fraction of the gas,  $a_{\text{cl}}$ , be contained in cold, dense clouds. The remaining fraction of the gas,  $(1 - a_{\text{cl}})$ , is distributed diffusely using the Dickey-Lockman density distribution (Dickey & Lockman 1990). We consider two cloud geometries: (1) spheres of radius  $r_{\text{cl}}$ ; or (2) cylindrical disks with radius  $r_{\text{cl}}$  and an aspect ratio  $\delta_p = h/r_{\text{cl}}$ , where  $h < r_{\text{cl}}$  is the height of the cylinder. Each of the cylindrical disks is assumed to be “face-on” with respect to the line of sight from the OB association. For either geometry, all clouds are assumed to have identical column densities, sizes, and densities. The number of clouds per unit area of the disk is given by

$$N_{\text{cl}} = \frac{a_{\text{cl}} N_{\text{HI}}}{V_{\text{cl}} n_{\text{cl}}}, \quad (28)$$

where  $V_{\text{cl}}$  is the volume of each cloud,  $n_{\text{cl}}$  is the density of hydrogen within each cloud, and  $N_{\text{HI}} = 6 \times 10^{20} \text{ cm}^{-2}$  is the observed total column density of hydrogen through the entire disk at the solar circle.

We assume that the clouds are distributed randomly within the disk of the galaxy using a probability distribution,  $P_{\text{cl}}(Z)$ , that is constant in the plane and proportional to

the Dickey-Lockman density distribution in the vertical direction. The *average* number of clouds intersecting a line of sight having an inclination angle  $\theta$  ( $\mu = \cos \theta$ ), emanating from an OB association situated on the midplane, is given by

$$N_{int} = \frac{\pi r_{cl}^2 N_{cl}}{2\mu} = \begin{cases} \frac{1.6}{\mu} \left(\frac{a_{cl}}{0.5}\right) \left(\frac{r_{cl}}{10 \text{ pc}}\right)^{-1} \left(\frac{n_{cl}}{30 \text{ cm}^{-3}}\right)^{-1} \left(\frac{\delta_p}{0.1}\right)^{-1} & : \text{ for cylindrical disks} \\ \frac{0.12}{\mu} \left(\frac{a_{cl}}{0.5}\right) \left(\frac{r_{cl}}{10 \text{ pc}}\right)^{-1} \left(\frac{n_{cl}}{30 \text{ cm}^{-3}}\right)^{-1} & : \text{ for spheres} \end{cases} \quad (29)$$

As in §2.3.2, the fraction of LyC photons from a single OB association that escape each side of the disk is given by

$$\eta_{esc}(S) = \int_0^{\pi/2} \frac{f(\theta, S)}{2} \sin(\theta) d\theta, \quad (30)$$

where

$$f(\theta, S) = 1 - \frac{4\pi\alpha_H^{(2)}}{S} \int_0^\infty n_H^2(r) r^2 dr. \quad (31)$$

Here,  $n_H(r)$  is given by the diffuse density distribution for radii outside any cloud and is equal to  $n_{cl}$  for radii inside any cloud. For a given value of  $\theta$  and  $S$ , we evaluate  $f(\theta, S)$  by averaging over 100 Monte-Carlo simulations. For each simulation, the number of clouds along the line of sight is drawn from a Poisson distribution having an average number of clouds given by equation (29). The distances from the origin of each of these clouds to the OB association are picked randomly using the probability distribution  $P_{cl}(Z)$ . For spherical clouds, the average chord length between the line of sight and the cloud is  $l = h = 4r_{cl}/3$ . For the cylindrical clouds, we assume that each cloud is orientated face-on, such that  $l = \delta_p r_{cl}$ . The observed column density of each cloud in the line of sight is  $n_{cl}l$ . Using the average values of  $f(\theta, S)$ , we determine  $\eta_{esc}(S)$  via equation (30). Finally, as in DS94, we determine the total fraction of ionizing radiation that escapes the disk is determined by integrating over the luminosity function,

$$\langle f_{esc} \rangle = 2 \frac{\int_{S_1}^{S_2} \eta_{esc}(S) \frac{dN_{as}}{dS} dS}{\int_{S_1}^{S_2} \frac{dN_{as}}{dS} dS}. \quad (32)$$

In Table 1, we give  $\langle f_{esc} \rangle$  for various values of  $a_{cl}$ ,  $r_{cl}$ , and  $\delta_p$ . It is apparent that  $\langle f_{esc} \rangle$  is sensitive to these parameters, which are poorly constrained observationally. For a given

Table 1.  $\langle f_{\text{esc}} \rangle$  for Clumpy Static ISM

Geometry	$r_{\text{cl}}$ (pc)	$a_{\text{cl}}$	$\delta_{\text{p}}$	$S_2$ ( $10^{49} \text{ s}^{-1}$ )	$\langle f_{\text{esc}} \rangle$
disk	5	0.1	0.05	100	0.01
disk	5	0.1	0.05	250	0.03
disk	5	0.1	0.05	500	0.05
disk	5	0.1	0.10	100	0.03
disk	5	0.1	0.10	250	0.05
disk	5	0.1	0.10	500	0.08
disk	5	0.3	0.10	100	0.002
disk	5	0.3	0.10	250	0.006
disk	5	0.3	0.10	250	0.01
disk	10	0.3	0.05	100	0.04
disk	10	0.3	0.05	250	0.07
disk	10	0.3	0.05	500	0.09
disk	10	0.3	0.10	100	0.07
disk	10	0.3	0.10	250	0.10
disk	10	0.3	0.10	500	0.13
disk	10	0.5	0.10	100	0.05
disk	10	0.5	0.10	250	0.07
disk	10	0.5	0.10	500	0.09
sphere	5	0.3	0.05	100	0.15
sphere	5	0.3	0.05	250	0.20
sphere	5	0.3	0.05	500	0.23
sphere	10	0.3	0.05	100	0.18
sphere	10	0.3	0.05	250	0.23
sphere	10	0.3	0.05	500	0.27
sphere	10	0.5	0.1	100	0.23
sphere	10	0.5	0.1	250	0.29
sphere	10	0.5	0.1	500	0.33

value of  $a_{\text{cl}}$ ,  $\langle f_{\text{esc}} \rangle$  decreases as the average number of clouds within a line of sight increases. We find that the I-front is trapped within most clouds. Only clouds very close to the OB association are not able to trap the I-front and become completely ionized, a consequence of the high recombination rate within the cloud. Essentially all escaping radiation emanates from lines of sight that are free of clouds. For comparison, for the case where  $a_{\text{cl}} = 0$ ,  $\langle f_{\text{esc}} \rangle = 0.12, 0.18, 0.22$  for  $S_2(10^{49} \text{ s}^{-1}) = 100, 250, \text{ and } 500$ , respectively (these results are identical to those of DS94). We conclude that, if an appreciable amount of the H I gas is in cold clouds having a disk geometry and column densities and hydrogen densities similar to the H I clouds studied by Fitzpatrick & Spitzer (1997), then  $\langle f_{\text{esc}} \rangle$  can be a factor of  $\sim 2 - 5$  smaller than previously estimated. For a fixed amount of gas locked in cold clouds, spherical clouds occupy a smaller solid angle as compared to thin cylindrical clouds, allowing more radiation to escape. Note that, since we did not consider superbubbles in these calculations, these numbers are only indicative of the *relative* decrease of  $\langle f_{\text{esc}} \rangle$  when cold clouds are included in the model.

### 4.3. Poisoning

Although the survey used for calibrating the production rate of ionizing photons is heavily biased towards associations far away from the parent molecular cloud, most if not all associations were born in a molecular cloud. Therefore, early in the lifetime of the OB association, it is possible that a considerable amount of matter is photoablated from the molecular cloud. This material increases the interior density of the bubble, leading to radiative cooling, potentially at a rate equal to the the injected mechanical luminosity, a process independently dubbed “poisoning” by McKee (1986) and Shull & Saken (1995). This poisoning process can alter the evolution of a young superbubble, as well as the propagation of the I-front through the cavity.

To date, the photoablation rate has not been calculated for a time-varying luminosity of an OB cluster with a proper radiation spectrum. In addition, for a given mass-injection rate, solving the evolution of the injected gas within the cavity is a complex problem. These complexities lead to uncertainties in the radiative cooling rate, both in magnitude and in its time evolution. Therefore, in order to estimate the degree to which poisoning alters the evolution of the superbubble and  $\langle f_{\text{esc}} \rangle$ , we introduced a factor,  $g$ , representing the fraction of the mechanical luminosity injected into the cavity that is drained due to radiative cooling from both photoablated gas and evaporated gas from the dense shell. Thus,  $(1 - g)L_{\text{mech}}$  is the portion of energy available to do  $PdV$  work. In what we consider an extreme case, we let  $g = 0.5$  for the duration in which  $R_{sh}$  is less than 30 pc [see Shull

& Saken (1995) for a discussion of when cooling due to poisoning becomes negligible]. In this case, for our non-coeval model, we find that  $\langle f_{\text{esc}} \rangle$  increases by roughly 35%. This increase occurs because the superbubble shell expands more slowly, and the density of the shell is smaller (it is proportional to the Mach number squared of the shell), and because the column density of the shell increases more slowly.

On the other hand, it is possible that enough material is photoablated into the hot cavity that, after recombining, it contributes to the absorption of ionizing radiation emitted by the OB association, partially offsetting the increase in  $\langle f_{\text{esc}} \rangle$  due to the slower shell expansion. However, to model this process requires a knowledge of the relative configurations of the molecular cloud, the OB association, and the disk of the Galaxy. Also, the evolution of the injected gas, especially the expansion of the gas as it expands from the molecular cloud or shell boundaries and into the the line-of-sight between the OB association and the halo, is a numerical problem beyond the scope of this paper.

#### 4.4. Triggered Star Formation

The fraction of ionizing radiation escaping the H I disk would be increased if an appreciable number of OB associations were formed within pre-existing dynamic chimneys. The two-dimensional filling factor of dynamic chimneys is estimated by

$$f_{\text{fill}} \sim f_{\text{as}} \dot{N}_{\text{as}} \tau_{\text{ca}} \pi R_{\text{cy}}^2, \quad (33)$$

where  $f_{\text{as}}$  is the fraction of OB associations that are large enough to produce a dynamic chimney,  $\tau_{\text{ca}}$  is the lifetime of the cavity, and  $R_{\text{cy}}$  is the radius of the cavity. As discussed in §4.1, associations having an average mechanical luminosity  $L_{\text{mech}} \gtrsim 4 \times 10^{38} \text{ erg s}^{-1}$  are thought to be capable of blowing out of the Galactic disk (Mac Low & Ferrara 1999; Koo & McKee 1992). This corresponds to an OB association size of  $N_{\text{T}} \gtrsim 400$ , or a peak luminosity  $S_0 \gtrsim S_{\text{cr}} = 5 \times 10^{50} \text{ s}^{-1}$ . The fraction of associations that produce a dynamic chimney is then

$$f_{\text{as}} = \frac{\int_{S_{\text{cr}}}^{S_2} dN/dS_0}{\int_{S_1}^{S_2} dN/dS_0} = \frac{\left(\frac{S_2}{S_{\text{cr}}}\right)^{\Gamma-1} - 1}{\left(\frac{S_2}{S_1}\right)^{\Gamma-1} - 1} \approx \left(\frac{S_1}{S_{\text{cr}}}\right)^{\Gamma-1}, \quad (34)$$

where we assumed  $S_2 \gg S_{\text{cr}} \gg S_1$ . For  $\Gamma = 2$  and  $S_1 = 1 \times 10^{48} \text{ s}^{-1}$ ,  $f_{\text{as}} \approx 2 \times 10^{-3}$ . The lifetime of the dynamic chimney is estimated to be the sound crossing time,

$$\tau_{\text{ch}} \sim \frac{R_{\text{cy}}}{c_{\text{s}}} \sim 35 \left(\frac{10 \text{ km s}^{-1}}{c_{\text{s}}}\right) \left(\frac{\sigma_{\text{h}}}{0.18 \text{ kpc}}\right) \text{ Myr}. \quad (35)$$



Therefore, the probability that an OB association is born within a dynamic chimney is given by

$$f_{\text{fill}} \sim 0.18 \left( \frac{\dot{N}_{\text{as}}}{6.4 \text{ Myr kpc}^{-2}} \right) \left( \frac{\tau_{\text{as}}}{35 \text{ Myr}} \right) \left( \frac{R_{\text{cy}}}{2\sigma_{\text{h}}} \right)^2, \quad (36)$$

and it is unlikely that  $\langle f_{\text{esc}} \rangle$  is enhanced significantly by this process if OB associations are born randomly in space. However, as suggested by McCray & Kafatos 1987, the birth of OB associations could be triggered by the passage of the shock wave associated with another superbubble. Indeed, recent far ultraviolet, H $\alpha$ , and H I observations of several dwarf galaxies show evidence of secondary star-formation sites on the dense H I rims of superbubbles (Voit 1988; Stewart 1998).

## 5. Discussion and Conclusions

We find that  $\langle f_{\text{esc}} \rangle \sim 12\text{--}20\%$  for the coeval star-formation history and  $\langle f_{\text{esc}} \rangle \sim 4\text{--}10\%$  for the Gaussian star-formation history. For  $S_2 = 2 \times 10^{51} \text{ s}^{-1}$ ,  $\beta = 1$ , and  $\Gamma = 2$ , we obtain  $\langle f_{\text{esc}} \rangle = 13\%$  for the coeval SFH and  $\langle f_{\text{esc}} \rangle = 6\%$  for the Gaussian SFH. Adopting a production rate <sup>1</sup>,  $\Psi_{\text{LyC}} = 4.95 \times 10^7 \text{ cm}^{-2} \text{ s}^{-1}$ , the corresponding photon fluxes are  $\Phi_{\text{LyC}} = 2.1 \times 10^6 \text{ cm}^{-2} \text{ s}^{-1}$  for the coeval SFH and  $\Phi_{\text{LyC}} = 9.9 \times 10^5 \text{ cm}^{-2} \text{ s}^{-1}$  for the Gaussian SFH. For comparison,  $\langle f_{\text{esc}} \rangle = 15\%$  using the formalism of DS94, where the photon luminosity was assumed constant in time and dynamically evolving superbubbles were not considered. In order to determine the degree to which the differences between our new results and our old results are due to the treatment of expanding superbubbles and dynamic chimneys, we also calculated  $\langle f_{\text{esc}} \rangle$  for the case where we neglect entirely the superbubble dynamics but include the time-varying photon luminosities. For the same parameters as given above, we find  $\langle f_{\text{esc}} \rangle = 14\%$  for the Gaussian SFH and  $\langle f_{\text{esc}} \rangle = 16\%$  for the coeval SFH, values similar to the old model. These small differences are due solely to the new treatment of the luminosity function of associations with time-varying photon luminosities, as discussed in §3.3.1. Therefore, the inclusion of the evolution of superbubbles *reduces* the fraction of escaping radiation, as the superbubble shells trap more radiation. For coeval SFHs, the inclusion of the dynamics only changes  $\langle f_{\text{esc}} \rangle$  from 8.2% to 6.5%, since most radiation is emitted and escapes before a substantial shell has formed. On the other hand, for the Gaussian SFH,  $\langle f_{\text{esc}} \rangle$  drops from 14% to 6%. This reduction of  $\langle f_{\text{esc}} \rangle$  occurs

---

<sup>1</sup>This number is 50% higher than the value used in DS94, due to updated stellar atmosphere models whose yield of ionizing photons from OB associations is 50% higher than previously estimated (Sutherland & Shull 1999).

because the photon luminosity peaks after a shell has formed, causing fewer photons to escape compared to the case when superbubbles are neglected.

In DS94, we argued that  $\langle f_{\text{esc}} \rangle$  must be  $\sim 14\%$  in order for the Reynolds layer to be sustained by radiation from OB associations. However, using COSTAR model atmospheres, Sutherland & Shull (1999) found that the yield of ionizing photons from OB associations is 50% higher than previously estimated, and the production rate of ionizing photons by OB associations in the solar vicinity is  $\Phi_{\text{LyC}} = 4.95 \times 10^7 \text{ cm}^{-2} \text{ s}^{-1}$ . Thus, the required value of  $\langle f_{\text{esc}} \rangle$  to sustain the Reynolds layer is reduced to  $\langle f_{\text{esc}} \rangle \approx 8\%$ . The flux of escaping radiation for the Gaussian SFH is about 25% smaller than this required value. However, as discussed in §1, since a portion of the Reynolds layer may reside within the H I disk, it need not be sustained solely by the radiation escaping the disk.

Throughout this paper, we have assumed that the formation rate of OB associations is constant in time. For starburst galaxies, the observed star formation rate is much higher than the time-averaged value. Therefore, since  $\eta_{\text{esc}}(t)$  is at a maximum shortly after the formation of an OB association, starburst galaxies having a morphology similar to our Galaxy should have higher values of  $\langle f_{\text{esc}} \rangle$  than those predicted for our Galaxy. In addition, starburst galaxies may have lower H I column densities and lower gravitational fields, also contributing to a higher escape fraction of ionizing radiation. These considerations will be the focus of our subsequent work.

If OB associations are indeed the sources of radiation responsible for ionizing the Reynolds layer, it is possible that an appreciable amount of radiation can escape the Galaxy entirely and contribute to the intergalactic radiation field (Bechtold et al. 1987; Giroux & Shull 1997). If the average escape fraction from low-redshift, star-forming galaxies exceeds  $\sim 5\%$ , then the contribution of ionizing radiation to the intergalactic medium by galaxies can exceed the contribution for QSOs (Shull 1995; Madau & Shull 1996; Giallongo, Fontana & Madau 1997). We note, however, that our models predict only the flux of radiation penetrating the Galactic halo, before a portion of it is absorbed by the portion of the Reynolds layer situated high above the Galactic plane. In order to predict the fraction of radiation that escapes the Galaxy entirely, we need a self-consistent model of the density distribution of hydrogen gas within the halo, including the contribution due to high velocity clouds, whose covering fraction is uncertain. Murphy, Lockman, & Savage (1995) found that approximately 37% of 21-cm sightlines near quasars showed HVCs with  $N_{\text{HI}} \geq 7 \times 10^{17} \text{ cm}^{-2}$ . However, observations with the Parkes Multibeam Survey (Putman & Gibson 1999) show that the spatial distribution of H I in the HVCs is filamentary, suggesting that Lyman continuum could leak through. Furthermore, the actual HVC coverage fraction will vary considerably around the Galaxy, depending on proximity to spiral arms and upwelling

superbubbles.

For specificity, if we assume  $\langle f_{\text{esc}} \rangle = 0.06$ , then the upward ionizing flux is  $\Phi_{\text{LyC}} = 1.5 \times 10^6 \text{ cm}^{-2} \text{ s}^{-1}$  above the H I disk ( $Z \gtrsim 1 \text{ kpc}$ ). If this flux is incident on the HVCs, and if we use the relationship between H $\alpha$  emission and ionizing flux, for optically thick clouds and photoionization equilibrium (Bland-Hawthorn & Maloney 1999), then the predicted H $\alpha$  emission intensity is

$$I_E = 4.6 \text{ mR} \left( \frac{\Phi_{\text{LyC}}}{10^4 \text{ cm}^{-2} \text{ s}^{-1}} \right) = 0.69 \text{ R}. \quad (37)$$

This intensity is roughly a factor of two larger than the measured intensities from the Magellanic Stream (Weiner & Williams 1996) and the Smith HVC (Bland-Hawthorn et al. 1998).

In summary, we have shown that the escape fraction of ionizing radiation from star-forming regions of disk galaxies is strongly affected by the presence of superbubbles and a cloudy ISM. The shells of the expanding superbubbles quickly trap or attenuate the ionizing flux, so that most of the escaping radiation escapes shortly after the formation of the superbubble. In our models, the escape fraction above 1 kpc range from  $\langle f_{\text{esc}} \rangle \approx 3 - 20\%$ . For a Gaussian SFH,  $\langle f_{\text{esc}} \rangle$  is roughly a factor of two lower than the results of Dove & Shull (1994b), where superbubbles were not considered. If  $\langle f_{\text{esc}} \rangle \gtrsim 8\%$ , then the upward flux is sufficient to sustain the Reynolds layer. We have also examined the radiative transfer in a two-phase (cloud/intercloud) medium. We neglect the filling factor of hot, low-density gas, consistent with recent O VI studies. If a significant fraction of H I is distributed in cold clouds with  $n_{\text{H}} \sim 30 \text{ cm}^{-3}$  and column densities  $N_{\text{H}} \sim (10^{19} - 10^{20}) \text{ cm}^{-2}$ ,  $\langle f_{\text{esc}} \rangle$  can be reduced by a factor of  $\sim 2 - 5$  if the clouds have a disk geometry. Thus, the amount of ionizing photons that escape the disk into the IGM is likely to be highly variable, and will depend on the luminosity distribution of OB associations, the cloud structure, and the massive star formation history. If the escaping LyC radiation is ever observed directly, it will confirm these theoretical expectations but also verify the likelihood that stellar ionizing radiation plays an important role in reionization of the high-redshift IGM.

We thank Ralph Sutherland for the OB association luminosity curves. We thank Mark Giroux, Phil Maloney, John Bally, and Brad Gibson for informative discussions. We also thank the referee for useful suggestions that led to major improvements to the paper. This work was supported by the Astrophysical Theory Program at the University of Colorado, through grants NAG5-4063 from NASA and AST96-17073 from NSF.

## References

- Banfi, M., Rampazzo, R., Chincarini, G., & Henry, R. B. C. 1993, *A&A*, 280, 373
- Basu, S., Johnstone, D., & Martin, P. G. 1999, *ApJ*, 516, 843
- Bechtold, J., Weymann, R. J., Lin, Z., & Malkan, M. A. 1987, *ApJ*, 315, 180
- Bertschinger, E. 1986, *ApJ*, 304, 154
- Bland-Hawthorn, J. B., Veilleux, S., Cecil, G. N., Putman, M. E., Gibson, B. K., & Maloney, P. R. 1998, *MNRAS*, 299, 611
- Bland-Hawthorn, J. B., & Maloney, P. R. 1999, *ApJ*, 510, 33
- Blondin, J. M., Wright, E. B., Borkowski, K. J., & Reynolds, S. P. 1998, *ApJ*, 500, 342
- Bregman, J. N., & Harrington, J. P. 1986, *ApJ*, 309, 833
- Castor, J., McCray, R., & Weaver, R. 1975, *ApJ*, 200, L107
- Couchman, H. M. P., & Rees, M. J. 1986, *MNRAS*, 221, 53
- Dickey, J. M., & Lockman, F. J. 1990, *ARA&A*, 28, 215
- Dove, J. B., & Shull, J. M. 1994a, *ApJ*, 423, 196
- Dove, J. B., & Shull, J. M. 1994b, *ApJ*, 430, 222, DS94
- Dove, J. B., Ferrara, A., & Shull, J. M. 1999, in preparation
- Elmegreen, B. G., & Lada, C. J. 1977, *ApJ*, 214, 725
- Fitzpatrick, E. L., & Spitzer, L. Jr. 1997, *ApJ*, 475, 623
- Garmany, C. D. 1998, in *Origins*, ed. C. Woodward, J. M. Shull, H. A. Thronson, ASP Conference Series, Vol. 148, 184
- Giallongo, E., Fontana, A., & Madau, P. 1997, *MNRAS*, 289, 629
- Giroux, M. L., & Shull, J. M. 1997, *AJ*, 113, 1505
- Heiles, C. 1979, *ApJ*, 229, 533
- Kennicutt, R. C., Jr., Edgar, B. K., & Hodge, P. W. 1989, *ApJ*, 337, 761
- Kompaneets, A. S. 1960, *Sov. Phys. Dokl.*, 5, 46
- Koo, B.-C., & McKee, C. F. 1992, *ApJ*, 388, 93

- Lockman, F. J., Hobbs, L. M., & Shull, J. M. 1986, *ApJ*, 301, 380
- Mac Low, M.-M., & Ferrara, A. 1999, *ApJ*, 513, 142
- Mac Low, M.-M., & McCray, R. 1988, *ApJ*, 324, 776
- Mac Low, M.-M., McCray, R., & Norman, M. L. 1989, *ApJ*, 337, 141
- MacLow, M.-M., & Norman, M. L. 1993, *ApJ*, 407, 207
- Madau, P., & Shull, J. M. 1996, *ApJ*, 457, 551
- Massey, P., 1998, in *New Views of the Magellanic Clouds*, IAU Symp. 190, eds. Chu, Y.-W. et al., p. 14
- Mathis, J. S. 1986, *ApJ*, 301, 423
- McCray, R., & Kafatos, M. 1987, *ApJ*, 317, 190
- McCray, R., & Snow, T. P. 1979, *ARA&A*, 17, 213
- McKee, C. F. 1986, *Ap&SS*, 118, 383
- McKee, C. F., & Williams, J. P. 1997, *ApJ*, 476, 144
- Mezger, P. G. 1978, *A&A*, 70, 565
- Miller, W. W., I., & Cox, D. P. 1993, *ApJ*, 417, 579
- Mineshige, S., Shibata, K., & Shapiro, P. R. 1993, *ApJ*, 409, 663
- Murphy, E. M., Lockman, F. J., & Savage, B. D. 1995, *ApJ*, 447, 642
- Newman, W. I., Symbalisty, E. M. D., Ahrens, T. J., & Jones, E. M. 1999, *Icarus*, 138, 224
- Ostriker, J. P., & Cowie, L. L. 1981, *ApJ*, 243, L127
- Ostriker, J. P., & McKee, C. F. 1988, *Rev. Mod. Phys.*, 60, 1
- Putman, M. E., & Gibson, B. K. 1999, in *Stromlo Workshop on High-Velocity Clouds*, ed. B. K. Gibson & M. E. Putman, ASP Conf. Series, Vol 166, 276
- Reynolds, R. J. 1984, *ApJ*, 282, 191
- Reynolds, R. J. 1991a, *ApJ*, 372, L17
- Reynolds, R. J. 1991b, in *The Interstellar Disk-Halo Connection in Galaxies*, ed. H. Bloemen, (Dordrecht: Kluwer), 67
- Rozas, M., Beckman, J. E., & Knapen, J. H. 1996, *A&A*, 307, 735

- Shull, J. M., & Saken, J. M. 1995, *ApJ*, 444, 663
- Shull, J. M. 1995, in *Airborne Astronomy Symposium on the Galactic Ecosystem: From Gas to Stars to Dust*, ed. M. R. Haas, J. A. Davidson, E. F. Erickson, *ASP Conf. Series*, Vol. 73, 365
- Stewart, S. G. 1998, *IAU Circ.* 5302
- Sutherland, R. S., & Shull, J. M. 1999, in preparation
- Tomisaka, K. 1998, *MNRAS*, 298, 797
- Tomisaka, K., & Ikeuchi, S. 1986, *Pub. Astr. Soc. Japan*, 38, 697
- Vishniac, E. J. 1983, *ApJ*, 274, 152
- Vishniac, E. J. 1994, *ApJ*, 428, 186
- Voit, G. M. 1988, *ApJ*, 331, 343
- Weaver, R., McCray, R., Castor, J., Shapiro, P., & Moore, R. 1977, *ApJ*, 218, 317
- Weiner, B. J. & Williams, T. B. 1996, *AJ*, 111, 1156